

RESEARCH ARTICLE SUMMARY

NEURODEGENERATION

Combined adult neurogenesis and BDNF mimic exercise effects on cognition in an Alzheimer's mouse model

Se Hoon Choi, Enjana Bylykbashi, Zena K. Chatila, Star W. Lee, Benjamin Pulli, Gregory D. Clemenson, Eunhee Kim, Alexander Rompala, Mary K. Oram, Caroline Asselin, Jenna Aronson, Can Zhang, Sean J. Miller, Andrea Lesinski, John W. Chen, Doo Yeon Kim, Henriette van Praag, Bruce M. Spiegelman, Fred H. Gage, Rudolph E. Tanzi*

INTRODUCTION: Alzheimer's disease (AD) is the most common form of age-related dementia, characterized by cognitive impairment, neurodegeneration, β -amyloid ($A\beta$) deposition, neurofibrillary tangle formation, and neuroinflammation. The most popular therapeutic approach aimed at reducing $A\beta$ burden has not yet proved effective in halting disease progression. A successful therapy would both remove the pathological hallmarks of the disease and provide some functional recovery. The hippocampus contains neural progenitor cells that continue to generate new neurons, a process called adult hippocampal neurogenesis

(AHN). AHN is impaired before the onset of classical AD pathology in AD mouse models. Human AHN has also been reported to be altered in AD patients. However, evidence supporting a role for AHN in AD has remained sparse and inconclusive.

RATIONALE: Two fundamental questions remain: (i) whether AHN could be enhanced and exploited for therapeutic purposes for AD, and (ii) whether AHN impairment mediates aspects of AD pathogenesis. To address these questions, we increased AHN genetically (WNT3) and pharmacologically (P7C3) in AD transgenic

5 \times FAD mice and explored whether promoting AHN alone can ameliorate AD pathology and behavioral symptoms. We assessed the role of exercise, a known neurogenic stimulus, and explored whether promoting AHN in conjunction with the salutary biochemical changes induced by exercise can improve AD pathology and behavioral symptoms in mice. We also investigated whether AHN suppression, by irradiation, temozolomide, or dominant-negative WNT, contributes to AD pathogenesis and assessed the functional roles of AHN in AD.

RESULTS: Inducing AHN alone conferred minimal to no benefit for improving cognition in 5 \times FAD mice. Exercise-induced AHN improved cognition along with reduced $A\beta$ load and increased levels of brain-derived neurotrophic factor (BDNF), interleukin-6

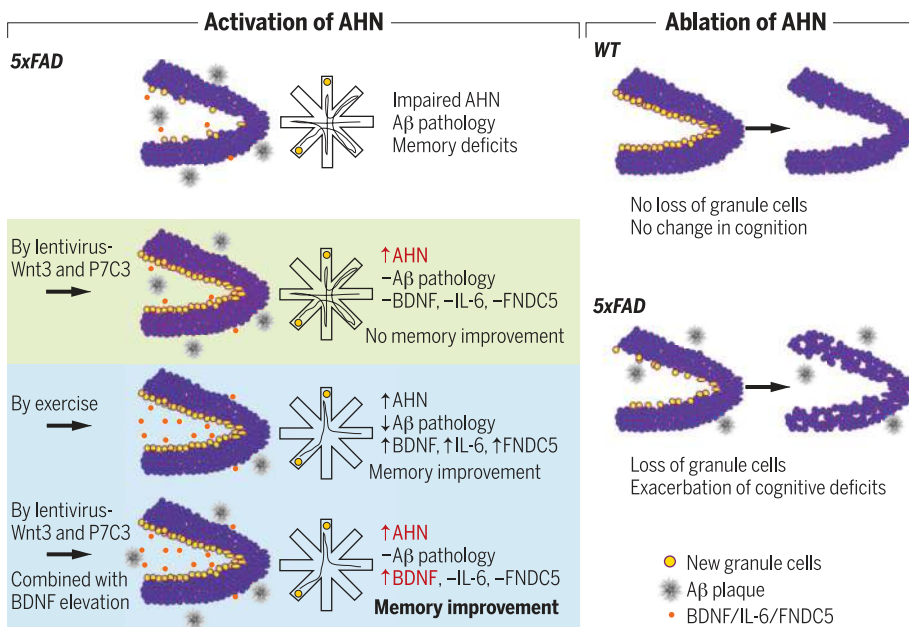
ON OUR WEBSITE

Read the full article at <http://dx.doi.org/10.1126/science.aan8821>

(IL-6), fibronectin type III domain-containing protein-5 (FNDC5), and synaptic markers. However, AHN activation was also required for exercise-induced

improvement in memory. Inducing AHN genetically and pharmacologically in combination with elevating BDNF levels mimicked beneficial effects of exercise on AD mice. Conversely, suppressing AHN in early stages of AD exacerbated neuronal vulnerability in later stages of AD, leading to cognitive impairment and increased neuronal loss. However, no such effects from AHN ablation were observed in nontransgenic wild-type (WT) mice, suggesting that AHN has a specific role in AD.

CONCLUSION: Promoting AHN can only ameliorate AD pathology and cognitive deficits in the presence of a healthier, improved local brain environment, e.g., stimulated by exercise. Increasing AHN alone combined with overexpression of BDNF could mimic exercise-induced improvements in cognition, without reducing $A\beta$ burden. Adult-born neurons generated very early in life are critical for maintaining hippocampal neuronal populations in the hostile brain environment created by AD later in life. Thus, AHN impairment may be a primary event that later mediates other aspects of AD pathogenesis. Future attempts to create pharmacological mimetics of the benefits of exercise on both increased AHN and BDNF may someday provide an effective means for improving cognition in AD. Moreover, increasing neurogenesis in the earliest stages of AD pathogenesis may protect against neuronal cell death later in the disease, providing a potentially powerful disease-modifying treatment strategy for AD. ■



Role of adult-born neurons in AD. Inducing AHN alone by WNT3 and P7C3 together did not prevent cognitive dysfunction, whereas activating AHN through exercise improved memory in 5 \times FAD mice. Increasing AHN alone together with overexpression of BDNF could mimic exercise-induced improvement in cognition. Suppressing AHN exacerbated neuronal vulnerability, leading to cognitive impairment and increased neuronal loss in 5 \times FAD mice, but not in WT mice.

The list of author affiliations is available in the full article online.
*Corresponding author. Email: tanzi@helix.mgh.harvard.edu
Cite this article as S. H. Choi *et al.*, *Science* 361, eaan8821 (2018). DOI: [10.1126/science.aan8821](https://doi.org/10.1126/science.aan8821)

RESEARCH ARTICLE

NEURODEGENERATION

Combined adult neurogenesis and BDNF mimic exercise effects on cognition in an Alzheimer's mouse model

Se Hoon Choi¹, Enjana Bylykbashi¹, Zena K. Chatila^{1*}, Star W. Lee^{2†}, Benjamin Pulli³, Gregory D. Clemenson^{2‡}, Eunhee Kim¹, Alexander Rompala¹, Mary K. Oram¹, Caroline Asselin¹, Jenna Aronson^{1§}, Can Zhang¹, Sean J. Miller^{1||}, Andrea Lesinski^{1¶}, John W. Chen³, Doo Yeon Kim¹, Henriette van Praag⁴, Bruce M. Spiegelman⁵, Fred H. Gage², Rudolph E. Tanzi^{1#}

Adult hippocampal neurogenesis (AHN) is impaired before the onset of Alzheimer's disease (AD) pathology. We found that exercise provided cognitive benefit to 5×FAD mice, a mouse model of AD, by inducing AHN and elevating levels of brain-derived neurotrophic factor (BDNF). Neither stimulation of AHN alone, nor exercise, in the absence of increased AHN, ameliorated cognition. We successfully mimicked the beneficial effects of exercise on AD mice by genetically and pharmacologically inducing AHN in combination with elevating BDNF levels. Suppressing AHN later led to worsened cognitive performance and loss of preexisting dentate neurons. Thus, pharmacological mimetics of exercise, enhancing AHN and elevating BDNF levels, may improve cognition in AD. Furthermore, applied at early stages of AD, these mimetics may protect against subsequent neuronal cell death.

Alzheimer's disease (AD) is the most common form of age-related dementia, characterized by cognitive impairment, neurodegeneration, deposition of β -amyloid ($A\beta$), neurofibrillary tangle formation, and neuroinflammation (1). The most popular therapeutic approach aimed at reducing $A\beta$ burden has not yet proved effective in halting disease progression. A successful therapy would ideally both remove the pathological hallmarks of the disease and provide a level of functional recovery.

The human hippocampus contains neural progenitor cells (NPCs) that continue to generate new neurons, a process called adult hippocampal neurogenesis (AHN) (2). Although adult-generated neurons play an important role in learning and memory under physiological conditions, their function under pathological conditions, such as those of AD, has remained elusive. Emerging evidence indicates that AHN is impaired prior to the onset of classical AD pathology in AD mouse models, e.g., $A\beta$ deposition (3). Human AHN has also been reported to be altered in AD patients (4–9).

To date, however, the evidence supporting a role for AHN in AD has remained sparse and inconclusive. Two fundamental questions remain: (i) whether AHN could be enhanced and exploited for therapeutic purposes for AD, and (ii) whether AHN impairment mediates aspects of AD pathogenesis or is a neuroadaptive response to the complex pathological events of the disease. We set out to address these two questions genetically and pharmacologically in 5×FAD mice (10). We also assessed the role of physical exercise, a known neurogenic stimulus that counteracts various aspects of AD pathology (11–13), and explored whether promoting AHN in conjunction with the salutary biochemical changes that are induced by exercise can ameliorate AD pathology and behavioral symptoms in mice. Finally, we investigated how impairment of AHN contributes to AD pathogenesis and assessed the functional

roles of adult-generated neurons in the pathological course of AD.

AHN stimulation with LV-Wnt3 and P7C3 or with exercise

To stimulate AHN, beginning at 2 months of age for 4 or 4.5 months, sedentary 5×FAD mice were injected with P7C3, a compound that enhances NPC survival (14). At the 3-month time point, these mice also received lentivirus expressing WNT3 protein (LV-Wnt3) to increase NPC proliferation (15) (Fig. 1, A and B). Control 5×FAD mice were injected with vehicle and lentivirus expressing green fluorescent protein (LV-GFP, referred to as “5×FAD^{CTL}” mice). As an alternative means of inducing AHN, we also tested the effects of exercise on a 5×FAD mice cohort. Successful promotion of AHN with P7C3 and LV-Wnt3 or with exercise was observed in the male and female 5×FAD mice, as determined by immunostaining for doublecortin (DCX)⁺ neurons (Fig. 1, C and D). After completing cognition tasks, mice with similar DCX⁺ cell counts among the 5×FAD mice treated with P7C3 and LV-Wnt3 and the exercised 5×FAD mice were selected for further study; we included all those with levels higher than the maximum level seen in 5×FAD^{CTL} mice (mice in dashed box in Fig. 1D; see table S1 for animal numbers in each experimental group and group arrangement explanations). From here on, we refer to the subsets of 5×FAD mice treated with P7C3 and LV-Wnt3 to promote AHN or exercised 5×FAD mice in the box in Fig. 1D as “5×FAD^{ProAHN}” and “5×FAD^{AHN(RUN)}” mice, respectively. Exercised 5×FAD mice with less than the maximum DCX⁺ cell count seen in 5×FAD^{CTL} mice were designated “5×FAD^{W^{AHN(RUN)}}” mice. Mice were sacrificed at the age of 6 to 6.5 months, when untreated 5×FAD mice showed cognitive deficits compared to nontransgenic wild-type mice (WT) mice (fig. S1). Endogenous neurogenic changes and AD pathologies observed in untreated 5×FAD mice, including our rationale for employing this mouse line, are described in figs. S2 and S3 and materials and methods.

We tested whether AHN stimulation by exercise versus P7C3 and LV-Wnt3 affected $A\beta$ plaque amounts. Immunostaining with anti- $A\beta$ antibody 3D6 showed that, whereas exercised mice exhibited a decreased $A\beta$ burden, activation of AHN alone (by P7C3 and LV-Wnt3) did not change $A\beta$ plaque amounts (Fig. 1, C and E). 5×FAD^{W^{AHN(RUN)}} mice also had a reduced $A\beta$ burden, suggesting that an effect due to exercise and not AHN alone contributed to changes in $A\beta$ burden after physical activity.

Increasing AHN alone did not ameliorate cognitive function in 5×FAD mice

We examined whether promoting AHN could ameliorate cognitive impairment in AD. We performed a delayed nonmatching to place (DNMP) task to measure spatial pattern separation, an eight-arm radial arm maze (RAM) to measure reference and retention memory, and a Y-maze to measure spatial working memory. Pattern separation, which is the formation of distinct

¹Genetics and Aging Research Unit, Department of Neurology, Massachusetts General Hospital, Harvard Medical School, Charlestown, MA 02129, USA. ²Laboratory of Genetics, The Salk Institute for Biological Studies, La Jolla, CA 92037, USA. ³Institute for Innovation in Imaging, Department of Radiology, Massachusetts General Hospital, Boston, MA 02114, USA. ⁴Department of Biomedical Science, Charles E. Schmidt College of Medicine, and Brain Institute, Florida Atlantic University, Jupiter, FL 33458, USA. ⁵Department of Cancer Biology, Dana-Farber Cancer Institute, Boston, MA 02115, USA.

*Present address: Department of Neuroscience, Columbia University, New York, NY 10036, USA. †Present address: Department of Evolution, Ecology, and Organismal Biology, University of California, Riverside, Riverside, CA 92521, USA. ‡Present address: Department of Neurobiology and Behavior, University of California, Irvine, Irvine, CA 92697, USA. §Present address: Department of Brain and Cognitive Sciences, Massachusetts Institute of Technology, Cambridge, MA, USA. ||Present address: Department of Neurology and Neurological Sciences, School of Medicine, Stanford University, Stanford, CA 94305, USA. ¶Present address: Cell and Molecular Biology, University of Rhode Island, Kingston, RI 02881, USA. #Corresponding author. Email: tanzi@helix.mgh.harvard.edu

representations of similar inputs, has been shown to require adult-generated neurons (16). Reduced ability to separate patterns (i.e., to recognize differences between very similar events) is one of the first behavioral deficits in patients with mild cognitive impairments, which often progress to AD (17). The other cognition types listed are well accepted to be hippocampus dependent; however, it remains unclear whether AHN contributes to these memory types. We used the RAM and Y-maze, which are routine methods to assess memory function in AD mice (18), to explore whether increasing AHN also ameliorates AD-associated cognitive impairment in 5x FAD mice.

In the DNMP task, male cohorts of 5x FAD^{ProAHN} and 5x FAD^{+AHN(RUN)} mice showed similar improvements in pattern separation compared to 5x FAD^{CTL} mice at 5.5 to 6 months of age (Fig. 2A, left graph). However, in female cohorts, 5x FAD^{ProAHN} mice failed to show improved pattern separation memory compared to 5x FAD^{CTL} mice, whereas 5x FAD^{+AHN(RUN)} mice showed improvement (Fig. 2A, right graph). Both male and female 5x FAD^{ProAHN} mice failed to show improved working memory in the Y-maze, whereas 5x FAD^{+AHN(RUN)} mice performed better (Fig. 2B and fig. S4). Male mice were tested in the RAM task. In the training trials of the task, all the groups showed a clear learning curve during the

5-day training session (Fig. 2C, left graph). However, whereas 5x FAD^{+AHN(RUN)} mice showed significantly improved reference memory compared to 5x FAD^{CTL} mice on days 2 and 3, 5x FAD^{ProAHN} mice failed to show improved memory. The performance of 5x FAD^{ProAHN} mice did not differ from that of 5x FAD^{CTL} mice. In the retention memory task, on day 8, 5x FAD^{ProAHN} mice again failed to show improved memory, whereas 5x FAD^{+AHN(RUN)} mice did (Fig. 2C, right graph). Our results suggest that increasing AHN alone was sufficient to improve pattern separation memory in male 5x FAD mice but not in female mice; however, it was not sufficient to improve other forms of cognition. By contrast, exercise

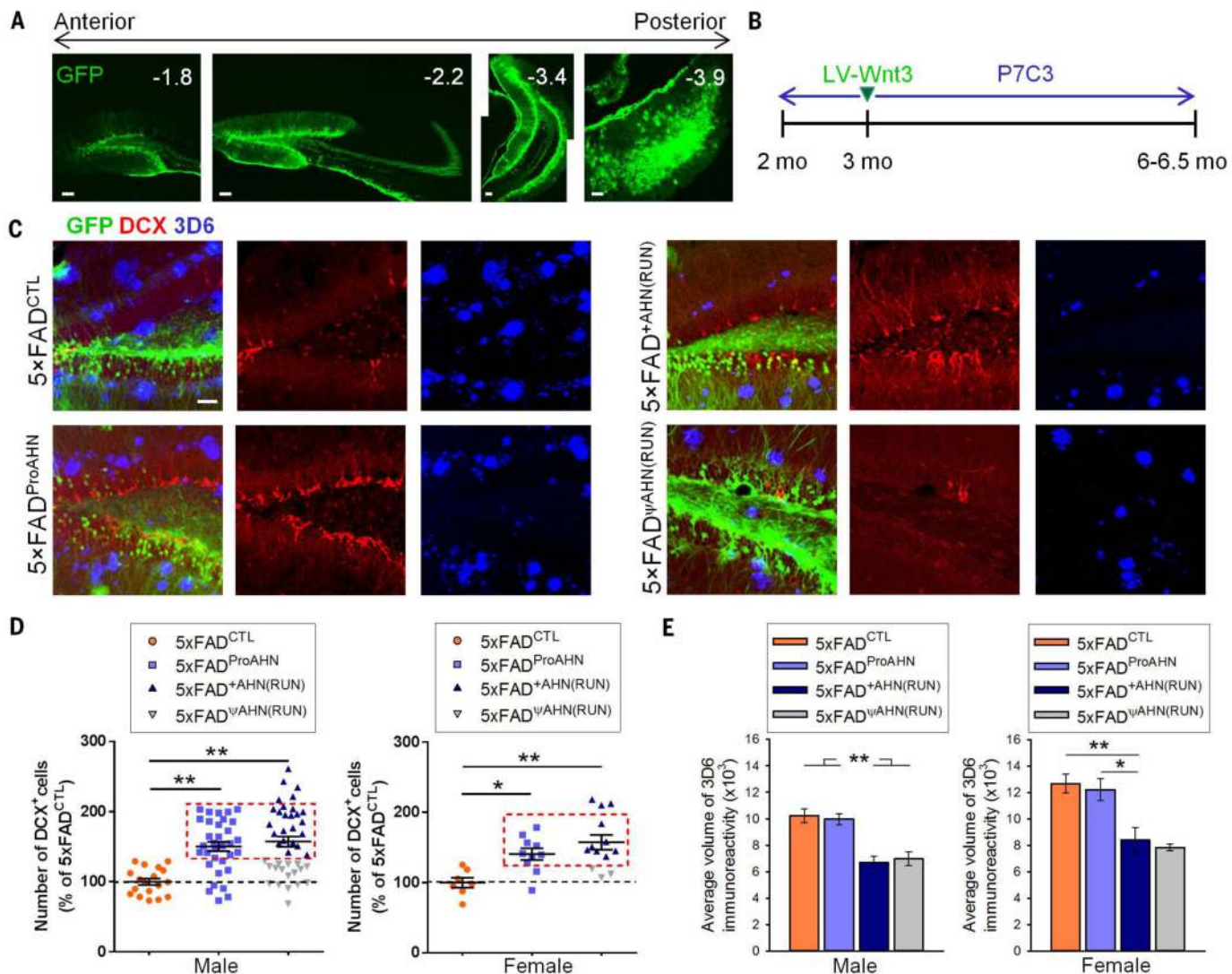


Fig. 1. AHN activation alone does not change A β plaque levels.

(A) Stereotaxic injection of lentiviral vectors targets adult DG. Numbers (upper right) are approximate distances from bregma. Scale bar: 100 μ m. (B) Experimental procedures timeline. (C) Photomicrographs of DCX⁺ cells and 3D6⁺ A β plaques in the hippocampus of 5x FAD^{CTL}, 5x FAD^{ProAHN}, 5x FAD^{+AHN(RUN)}, and 5x FAD^{wAHN(RUN)} mice. Scale bar: 50 μ m. (D) Distribution of AHN activation by P7C3 along with LV-Wnt3 or by exercise. Data points represent DCX⁺ cell count per mouse, as

percentage of mean DCX⁺ cell count for 5x FAD^{CTL} mice by gender. In male 5x FAD^{CTL}, 5x FAD^{ProAHN}, and 5x FAD^{ProAHN} mice, $F_{(2,90)} = 13.57$, $P < 0.01$. In female, $F_{(2,27)} = 8.05$, $P < 0.01$. (E) Quantitative analysis of A β burden volume in the hippocampus of 5x FAD^{CTL}, 5x FAD^{ProAHN}, 5x FAD^{+AHN(RUN)}, and 5x FAD^{wAHN(RUN)} mice. Volume in arbitrary units (mean voxel count \pm SEM; male, $F_{(3,76)} = 15.57$, $P < 0.01$; female, $F_{(2,19)} = 7.659$, $P < 0.01$). Female 5x FAD^{wAHN(RUN)} mice were excluded due to low n .

led to improved cognitive function in all three types of memory tests.

Interestingly, exercise alone, in the absence of increased AHN, exerted no observed beneficial effects on cognitive function ($5\times\text{FAD}^{\psi\text{AHN}(\text{RUN})}$, Fig. 2). This finding suggests that increased AHN above physiological levels is required for the positive behavioral effects of exercise in $5\times\text{FAD}$ mice. However, a lack of AHN in WT mice does not block the beneficial behavioral effects of increased physical activity gained through living in an enriched environment (19). We hypothesized that adult-generated neurons have specific functions in AD pathological conditions and in mediating the effects of exercise in AD. To test these points, we assessed the effects of AHN ablation in $5\times\text{FAD}$ mice versus WT mice.

Ablating AHN induced cell death in dentate gyrus (DG) of $5\times\text{FAD}$ mice

To block AHN, 6- to 8-week-old male WT and $5\times\text{FAD}$ mice received either focal irradiation (20) (IR; WT^{IR} ; $5\times\text{FAD}^{\text{IR}}$), the DNA-alkylating agent

temozolomide (21) (TMZ; WT^{TMZ} ; $5\times\text{FAD}^{\text{TMZ}}$), or a lentivirus expressing a dominant-negative form of WNT (15) (LV-dnWnt; $\text{WT}^{\text{LV-dnWnt}}$; $5\times\text{FAD}^{\text{LV-dnWnt}}$) (Fig. 3, A to C). They were then sacrificed at 3 or 5 months of age. Sham mice (WT^{Sham} ; $5\times\text{FAD}^{\text{Sham}}$) and mice treated with vehicle (WT^{Veh} ; $5\times\text{FAD}^{\text{Veh}}$) or LV-GFP ($\text{WT}^{\text{LV-GFP}}$; $5\times\text{FAD}^{\text{LV-GFP}}$) served as controls for mice treated with IR, TMZ, and LV-dnWnt, respectively. IR almost completely eliminated AHN, as determined by immunostaining for DCX⁺ neurons, in both WT and $5\times\text{FAD}$ mice. Injection of TMZ or LV-dnWnt also showed significant, although variable, AHN knockdown (Fig. 3C; see table S2 for animal numbers in each experimental group and group arrangement explanations).

To test whether adult-generated neurons are required to maintain stability in existing neuronal populations in AD, we stained brain sections from each group with an antibody against activated Caspase 3 (Casp3), a marker for apoptotic cells, and examined them for evidence of cell loss. $5\times\text{FAD}^{\text{Sham}}$, $5\times\text{FAD}^{\text{Veh}}$, and $5\times\text{FAD}^{\text{LV-GFP}}$

mice showed only a few Casp3⁺ cells in the DG at 5 months of age. Conversely, the number of Casp3⁺ cells was significantly increased in the DG of 5-month-old $5\times\text{FAD}^{\text{IR}}$, $5\times\text{FAD}^{\text{TMZ}}$, and $5\times\text{FAD}^{\text{LV-dnWnt}}$ mice; no such cell death was observed in the corresponding WT treatment groups (Fig. 3, D and E). However, $5\times\text{FAD}^{\text{TMZ}}$ and $5\times\text{FAD}^{\text{LV-dnWnt}}$ mice that showed less than ~60% AHN reduction did not exhibit a significant increase in the number of Casp3⁺ cells compared to $5\times\text{FAD}^{\text{Veh}}$ and $5\times\text{FAD}^{\text{LV-GFP}}$ mice, respectively (Fig. 3F). These results suggest that the existence of Casp3⁺ cells in $5\times\text{FAD}^{\text{TMZ}}$ and $5\times\text{FAD}^{\text{LV-dnWnt}}$ mice could be dependent on the degree of AHN knockdown.

Therefore, we regrouped $5\times\text{FAD}^{\text{TMZ}}$ mice based on the degree of AHN knockdown. $5\times\text{FAD}^{\text{TMZ}(\text{Mod KD})}$ showed moderate (less than 60% AHN reduction) and $5\times\text{FAD}^{\text{TMZ}(\text{high KD})}$ showed high (over 60% AHN reduction) AHN knockdown. Likewise, the $5\times\text{FAD}^{\text{LV-dnWnt}}$ group was regrouped into $5\times\text{FAD}^{\text{LV-dnWnt}(\text{Mod KD})}$ and $5\times\text{FAD}^{\text{LV-dnWnt}(\text{high KD})}$ mice. WT mice injected with TMZ or LV-dnWnt

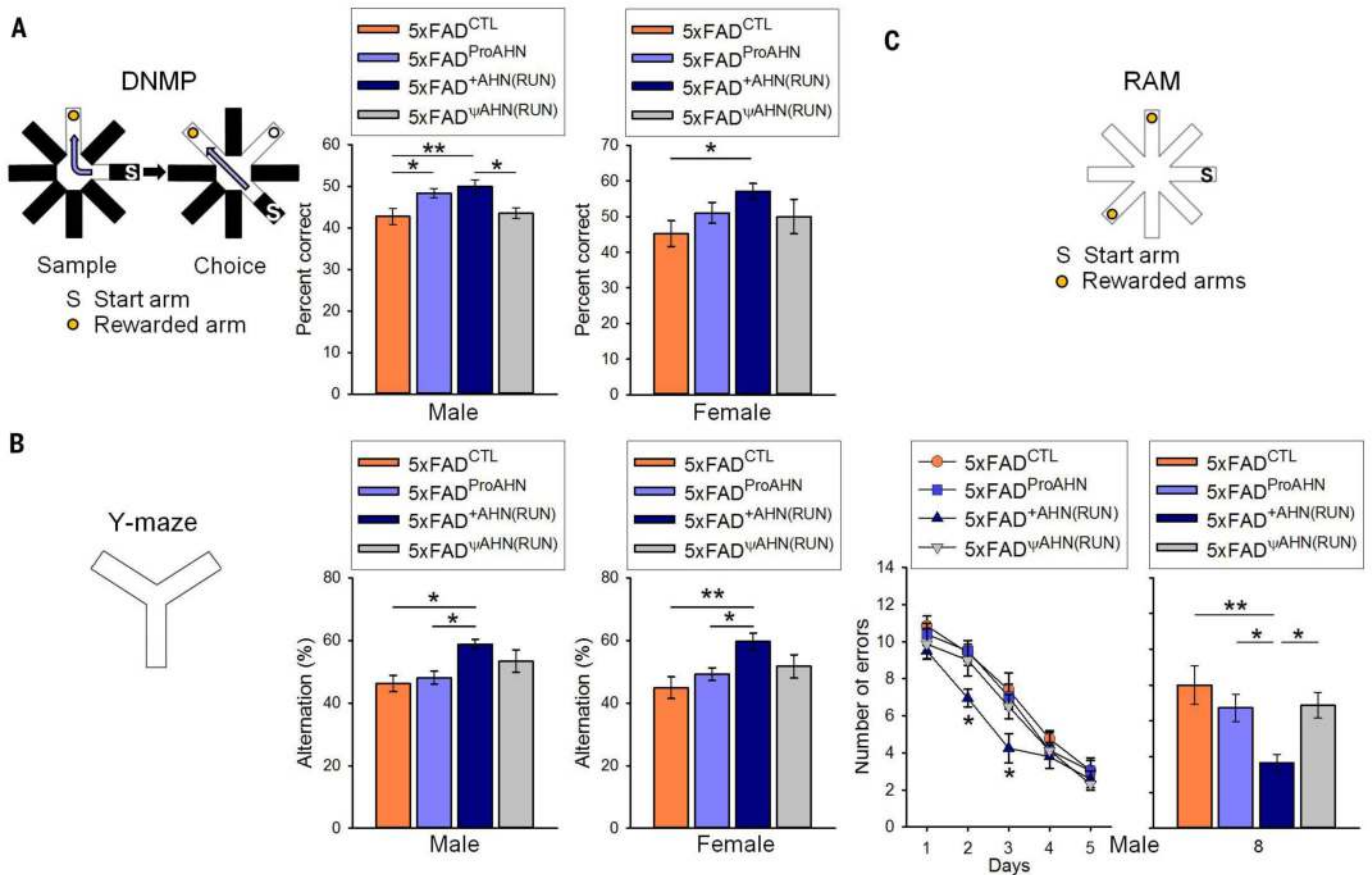


Fig. 2. Increasing AHN alone does not ameliorate cognitive function in $5\times\text{FAD}$ mice, whereas exercise-induced AHN does.

(A) Schematic of DNMP in the RAM task, which consisted of sample and choice phase, and quantification of percent correct during choice phase (male, $F_{(3,31)} = 5.983$, $P < 0.01$; female, $F_{(2,19)} = 3.887$, $P < 0.05$). (B) Schematic of Y-maze task and spontaneous alternation behavior (male, $F_{(3,31)} = 3.935$, $P < 0.05$; female, $F_{(2,19)} = 7.416$, $P < 0.01$). Total arm entries were comparable among groups (fig. S4). (C) Schematic of RAM task and

mean error number in training trials (left graph). Two-way ANOVA with repeated measures revealed significant effects for days ($F_{(4,164)} = 99.29$, $P < 0.01$) and groups ($F_{(3,41)} = 5.129$, $P < 0.01$) but not interaction ($F_{(12,164)} = 0.9894$, $P = 0.4613$). Analysis of error number on each day by Fisher's LSD post hoc tests revealed $5\times\text{FAD}^{\text{+AHN(RUN)}}$ differed significantly from both $5\times\text{FAD}^{\text{CTL}}$ and $5\times\text{FAD}^{\text{ProAHN}}$ mice on days 2 and 3 (day 2, $F_{(3,41)} = 4.074$, $P < 0.05$; day 3, $F_{(3,41)} = 3.499$, $P < 0.05$). Right graph: mean error number in memory retention trial ($F_{(3,41)} = 5.675$, $P < 0.01$).

were also regrouped into WT^{TMZ (Mod KD)} and WT^{TMZ (high KD)} groups, and WT^{LV-dnWnt (Mod KD)} and WT^{LV-dnWnt (high KD)} groups. As shown in Fig. 3F, 5×FAD^{TMZ (high KD)} mice showed significantly increased Casp3⁺ cell numbers compared to both 5×FAD^{Veh} and 5×FAD^{TMZ (Mod KD)} mice, whereas 5×FAD^{TMZ (Mod KD)} mice did not show increased Casp3⁺ cells compared to 5×FAD^{Veh} mice. Similarly, 5×FAD^{LV-dnWnt (high KD)} mice showed increased Casp3⁺ cell numbers compared to both 5×FAD^{LV-GFP} and 5×FAD^{LV-dnWnt (Mod KD)} mice, whereas no significant difference was observed

between 5×FAD^{LV-GFP} and 5×FAD^{LV-dnWnt (Mod KD)} mice.

From here on, 5×FAD^{Sham}, 5×FAD^{Veh}, and 5×FAD^{LV-GFP} mice are collectively referred to as 5×FAD^{CTL}; 5×FAD^{IR}, 5×FAD^{TMZ}, and 5×FAD^{LV-dnWnt} mice as 5×FAD^{AHN} mice; 5×FAD^{IR}, 5×FAD^{TMZ (High KD)}, and 5×FAD^{LV-dnWnt (High KD)} mice as 5×FAD^{AHN (High KD)} mice; 5×FAD^{TMZ (Mod KD)} and 5×FAD^{LV-dnWnt (Mod KD)} mice as 5×FAD^{AHN (Mod KD)} mice. Likewise, the corresponding groups of WT mice are referred to as WT^{CTL}, WT^{AHN}, WT^{AHN (High KD)}, and WT^{AHN (Mod KD)} mice, respectively.

Most Casp3⁺ cells were colabeled with NeuN, a mature neuronal marker (Fig. 4A), suggesting that AHN suppression caused the death of mature neurons. The total number of granule cells was decreased by the death of mature neurons in the 5×FAD^{AHN (High KD)} group but not in the WT^{AHN (High KD)} group (Fig. 4B), demonstrating the importance of AHN in the survival of the preexisting granule cell population. The number of granule cells was not decreased in 5×FAD^{AHN (Mod KD)} mice. Our results suggest that AHN plays a potential function in maintaining

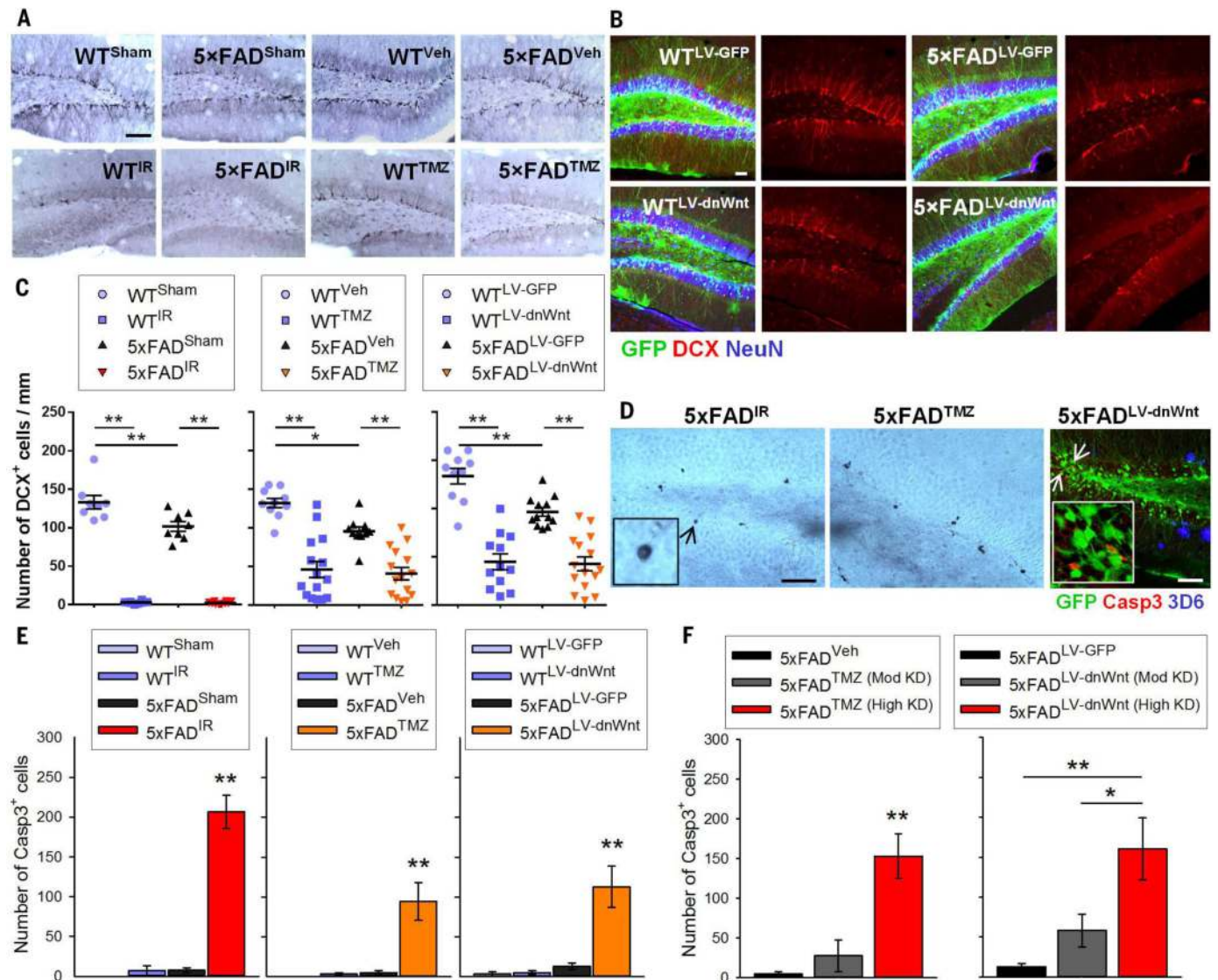


Fig. 3. Ablating AHN induces cell death in 5×FAD mice. (A) Photomicrographs of DCX⁺ cells in the DG of 5-month-old WT^{Sham}, 5×FAD^{Sham}, WT^{Veh}, 5×FAD^{Veh}, WT^{IR}, 5×FAD^{IR}, WT^{TMZ}, and 5×FAD^{TMZ} mice. Scale bar: 100 μm. (B) Photomicrographs of DCX⁺ cells in the transduced DG of WT and 5×FAD mice by LV-GFP or LV-dnWnt. Mature granule neurons are stained for NeuN. Scale bar: 50 μm. (C) Quantification of DCX⁺ cells in male WT^{Sham}, WT^{IR}, 5×FAD^{Sham}, and 5×FAD^{IR} ($F_{(3,32)} = 197.9$, $P < 0.01$; left), WT^{Veh}, WT^{TMZ}, 5×FAD^{Veh}, and 5×FAD^{TMZ} ($F_{(3,46)} = 23.96$, $P < 0.01$; middle), and WT^{LV-GFP}, WT^{LV-dnWnt}, 5×FAD^{LV-GFP}, and 5×FAD^{LV-dnWnt} mice ($F_{(3,45)} = 35.21$, $P < 0.01$; right). (D) Representative images of

Casp3⁺ cells in 5×FAD^{IR} (left), 5×FAD^{TMZ} (middle), or 5×FAD^{LV-dnWnt} (right) mice. Insets represent digital magnification of arrow-indicated Casp3⁺ cells. Scale bars: 50 μm. (E) Quantification of Casp3⁺ cells in WT^{Sham}, WT^{IR}, 5×FAD^{Sham}, and 5×FAD^{IR} ($F_{(3,32)} = 72.38$, $P < 0.01$; left), WT^{Veh}, WT^{TMZ}, 5×FAD^{Veh}, and 5×FAD^{TMZ} ($F_{(3,46)} = 11.26$, $P < 0.01$; middle), and WT^{LV-GFP}, WT^{LV-dnWnt}, 5×FAD^{LV-GFP}, and 5×FAD^{LV-dnWnt} mice ($F_{(3,45)} = 11.98$, $P < 0.01$; right). (F) Quantification of Casp3⁺ cells in 5×FAD^{Veh}, 5×FAD^{TMZ (Mod KD)}, and 5×FAD^{TMZ (High KD)} ($F_{(2,22)} = 19.41$, $P < 0.01$; left), and 5×FAD^{LV-GFP}, 5×FAD^{LV-dnWnt (Mod KD)}, and 5×FAD^{LV-dnWnt (High KD)} mice ($F_{(2,24)} = 12.17$, $P < 0.01$; right).

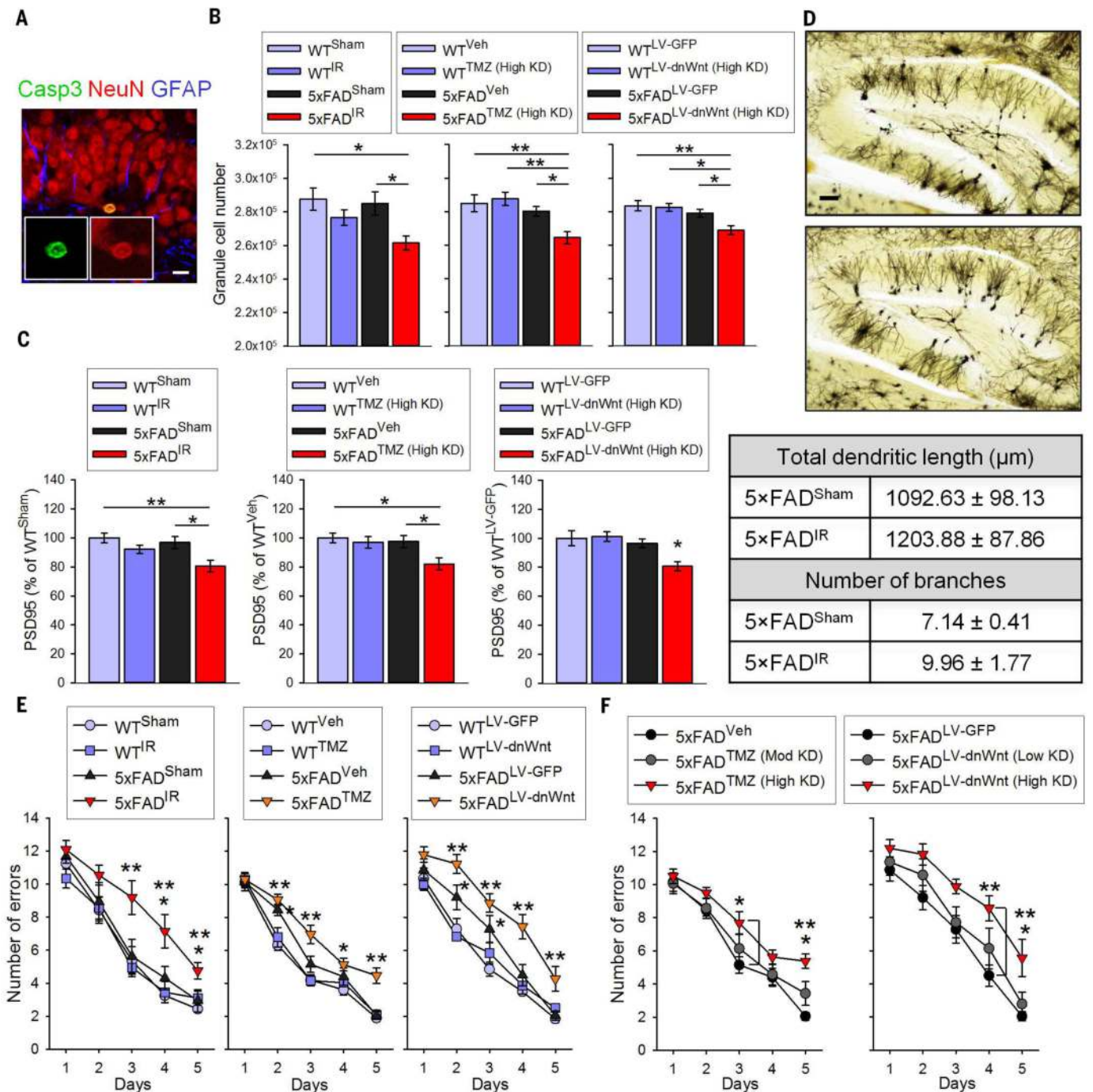


Fig. 4. Ablating AHN induces granule cell and synaptic marker loss, and exacerbates cognitive impairment in 5x FAD mice. (A) Representative images of Casp3⁺ cell colabeled with NeuN. Scale bar: 10 μm . (B) Quantification of granule cell number in WT^{Sham}, WT^{IR}, 5x FAD^{Sham}, and 5x FAD^{IR} mice ($F_{(3,32)} = 4.658, P < 0.01$; left); WT^{Veh}, WT^{TMZ} (High KD), 5x FAD^{Veh}, and 5x FAD^{TMZ} (High KD) mice ($F_{(3,33)} = 6.041, P < 0.01$; middle); and WT^{LV-GFP}, WT^{LV-dnWnt} (High KD), 5x FAD^{LV-GFP}, and 5x FAD^{LV-dnWnt} (High KD) mice ($F_{(3,33)} = 5.476, P < 0.01$; right). (C) Hippocampal PSD95 levels (left: $F_{(3,32)} = 5.753, P < 0.01$; middle: $F_{(3,33)} = 3.983, P < 0.05$; right: $F_{(3,33)} =$

4.639, $P < 0.01$). (D) Representative Golgi stains in 5x FAD^{Sham} (upper) and 5x FAD^{IR} (lower) mice, and quantification of total dendritic length and neuron branch number in outer granule cell layer of 5x FAD^{Sham} ($n = 3$) and 5x FAD^{IR} mice ($n = 4$). Scale bar: 100 μm . (E and F) Mean number of errors in training days of RAM task. In (E), left: WT^{Sham}, WT^{IR}, 5x FAD^{Sham}, and 5x FAD^{IR} mice; middle: WT^{Veh}, WT^{TMZ}, 5x FAD^{Veh}, and 5x FAD^{TMZ} mice; right: WT^{LV-GFP}, WT^{LV-dnWnt}, 5x FAD^{LV-GFP}, and 5x FAD^{LV-dnWnt} mice. In (F), left: 5x FAD^{Veh}, 5x FAD^{TMZ} (Mod KD), and 5x FAD^{TMZ} (High KD) mice; right: 5x FAD^{LV-GFP}, 5x FAD^{LV-dnWnt} (Mod KD), and 5x FAD^{LV-dnWnt} (High KD) mice.

the structural integrity of the DG specifically under pathological conditions of AD but not under normal physiological conditions.

Enzyme-linked immunosorbent assay (ELISA) and immunoblot assays revealed that the levels of postsynaptic density 95 (PSD95) and synapse-associated protein 97 (SAP97) in the hippocampal homogenates of 5x*FAD*^{AHN (High KD)} mice were reduced compared to 5x*FAD*^{CTL} mice at 5 months of age (Fig. 4C and fig. S5). Meanwhile, AHN reduction did not change the levels of PSD95 and SAP97 in WT mice. These results demonstrate that suppressing AHN resulted

in considerable loss of synaptic proteins PSD95 and SAP97 in the hippocampus of 5x*FAD* mice, likely due to DG neuronal cell death.

Golgi staining showed that the morphology of granule neurons in the outer granule cell layer, generated during early development, of 5x*FAD*^{IR} mice did not differ from that of neurons of 5x*FAD*^{Sham} mice (Fig. 4D and fig. S6). Furthermore, Casp3⁺ cell number did not increase in 5x*FAD*^{AHN (Mod KD)} mice (Fig. 3F). These results suggest that the increase in Casp3⁺ cells and loss of granule neurons and synaptic markers in 5x*FAD*^{AHN (High KD)} mice can be attributed

mostly to AHN loss, rather than the direct impact of IR, TMZ, or LV-dnWnt on the existing neurons in the more susceptible brain environment of 5x*FAD* mice.

Five-month-old 5x*FAD* mice in which AHN was suppressed much later (at 4 to 4.5 months), and which had AHN levels similar to those of untreated 5x*FAD* mice before AHN was suppressed, exhibited only negligible Casp3⁺ cell numbers (fig. S7A). We also could not detect any significant Casp3⁺ cell numbers in 3-month-old 5x*FAD* mice in which AHN was ablated starting at 1.5 to 2 months old (fig. S7B). These results indicate

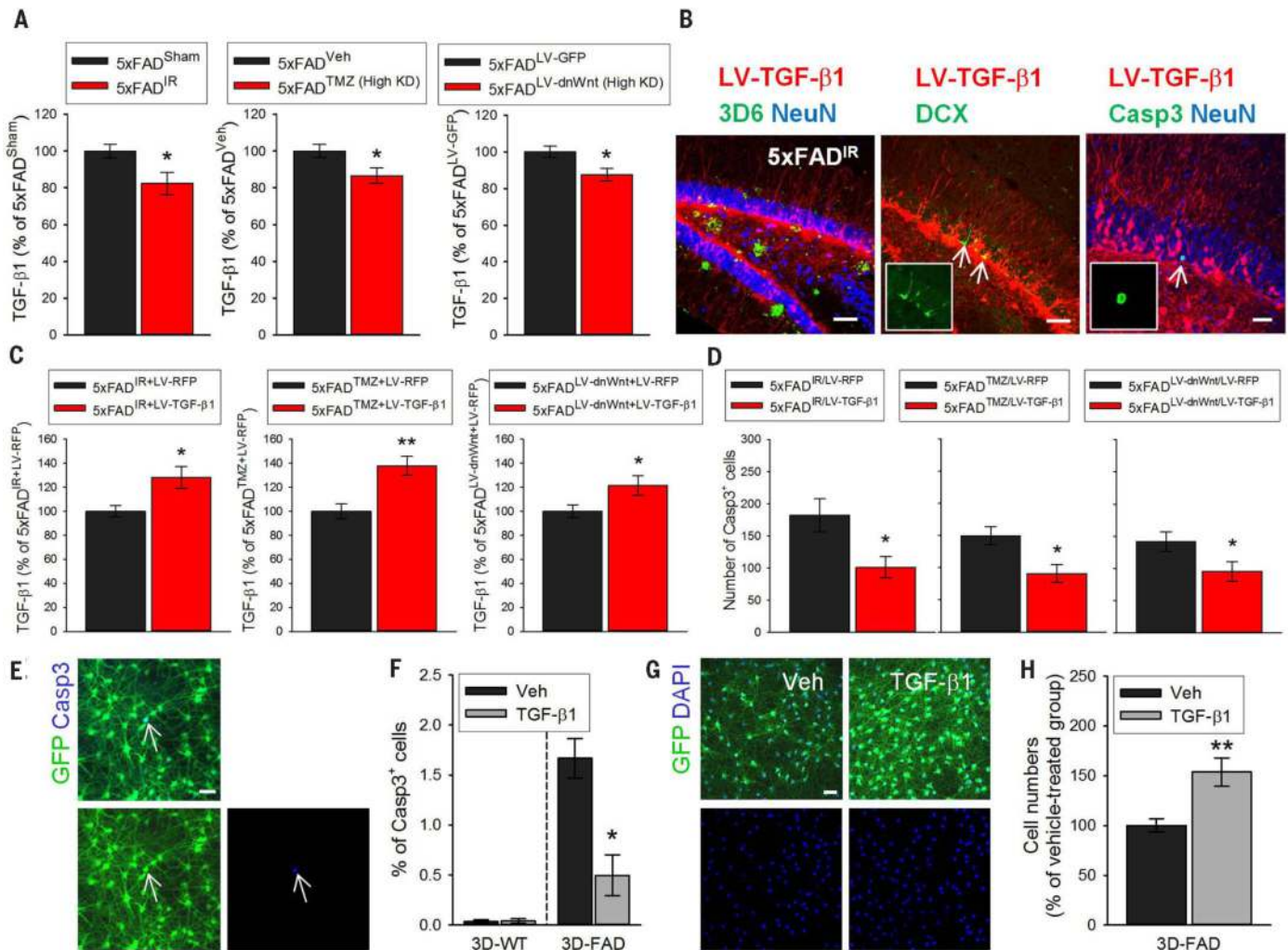


Fig. 5. Ablating AHN in male 5x*FAD* mice reduces hippocampal levels of TGF- β 1, a protective cytokine. (A) Hippocampal TGF- β 1 levels in male 5x*FAD*^{Sham} and 5x*FAD*^{IR} (left), 5x*FAD*^{Veh} and 5x*FAD*^{TMZ (High KD)} (middle), and 5x*FAD*^{LV-GFP} and 5x*FAD*^{LV-dnWnt (High KD)} mice (right). Levels are shown as percent of 5x*FAD* control group in each treatment. (B) Photomicrographs of 3D6⁺ A β plaques and NeuN⁺ cells (left), DCX⁺ cells (middle), and Casp3⁺ cell and NeuN⁺ cells (right) in the transduced DG of 5x*FAD*^{IR} mice by LV-TGF- β 1. Insets represent digitally magnified images of the DCX⁺ cells (arrows, middle) or Casp3⁺ cell (arrow, right). Scale bars: 50 μ m (left, middle); 20 μ m (right). (C) Hippocampal TGF- β 1 levels in 5x*FAD*^{IR/LV-RFP} ($n = 8$) and 5x*FAD*^{IR/LV-TGF- β 1} ($n = 8$) (left), 5x*FAD*^{TMZ/LV-RFP} ($n = 9$) and 5x*FAD*^{TMZ/LV-TGF- β 1} ($n = 12$) (middle), and 5x*FAD*^{LV-dnWnt/LV-RFP} ($n = 8$) and

5x*FAD*^{LV-dnWnt/LV-TGF- β 1} ($n = 9$) (right) mice. Levels are shown as percent of 5x*FAD* control group in each treatment. 5x*FAD*^{TMZ/LV-RFP} and 5x*FAD*^{LV-dnWnt/LV-RFP} mice with moderate AHN knockdown were not included. (D) Quantification of Casp3⁺ cells in 5x*FAD*^{IR/LV-RFP} and 5x*FAD*^{IR/LV-TGF- β 1} (left), 5x*FAD*^{TMZ/LV-RFP} and 5x*FAD*^{TMZ/LV-TGF- β 1} (middle), and 5x*FAD*^{LV-dnWnt/LV-RFP} and 5x*FAD*^{LV-dnWnt/LV-TGF- β 1} (right) mice. (E) Representative images of Casp3⁺ cells (arrows) in GFP-labeled 3D-FAD cell cultures. Scale bar: 50 μ m. (F) Quantification of Casp3⁺ cells in 3D-FAD cell cultures treated with vehicle (veh) or TGF- β 1 (10 ng/ml). $n = 3$ per group. (G) Representative images of DAPI⁺ cells (blue) in ReN-FAD cell cultures treated with vehicle or TGF- β 1. Scale bar: 50 μ m. (H) Number of cells survived in 3D-FAD cultures treated with vehicle or TGF- β 1. $n = 3$ per group.

that adult-generated neurons at a relatively early stage of AD (6 weeks to 4 months old) are critical for later maintaining the survival and stability of granule neurons (at 5 months and older). Thus, AHN impairment at a very early disease stage appears to initiate cell death in later stages, i.e., when the neuronal milieu becomes more hostile [e.g., elevated levels of A β pathology, interleukin-1 β (IL-1 β), tumor necrosis factor α (TNF α), and keratinocyte-derived chemokine (KC/GRO); reduced levels of brain-derived neurotrophic factor (BDNF); figs. S2 and S3]. Blocking AHN did not affect the levels of A β deposition, numbers of Iba1⁺ microglia, or GFAP⁺ astrocytes in the hippocampus of 5-month-old 5 \times FAD mice (fig. S8), suggesting that AHN in 5 \times FAD mice had no effect on A β pathology or gliosis.

Ablating AHN exacerbated cognitive impairment in 5 \times FAD mice

We next investigated whether cognitive dysfunction progressed more rapidly in the absence of AHN in 5 \times FAD mice. Untreated 5 \times FAD mice showed significant impairment in pattern separation at 5 months compared to age-matched WT mice, but not at 3 months of age (fig. S1). Therefore, the impact of AHN loss on pattern separation memory was studied in WT^{AHN} and 5 \times FAD^{AHN} mice at 3 months of age. In the DNMP task, both 3-month-old WT^{AHN} and 5 \times FAD^{AHN} mice exhibited equally poor performances; no further impairment was observed in the 5 \times FAD^{AHN} mice compared to WT^{AHN} mice (fig. S9). These results suggest that adult-generated neurons are required for pattern separation both in WT and 5 \times FAD mice. Thus, decreased AHN in AD is sufficient to cause impairment of this memory type, and other AD pathological factors are not required for this behavioral change.

In the RAM task, 5-month-old WT^{AHN} mice did not perform differently from WT^{CTL} mice, indicating that WT mice lacking AHN could still perform this task at a normal rate. However, ablating AHN in 5-month-old 5 \times FAD mice resulted in significant cognitive impairments (Fig. 4E; see table S3 for statistical analysis and group performance). However, 5 \times FAD^{AHN (Mod KD)} mice performed comparably with 5 \times FAD^{CTL} mice (Fig. 4F; see table S4 for statistical analysis and group performance). These results suggest that a high degree of AHN knockdown, accompanied by loss of granule cells and synaptic markers, exacerbates AD-associated cognitive impairment in 5 \times FAD mice. Similar results were observed in the Y-maze task except that 5 \times FAD^{LV-dnWnt (Mod KD)} mice also showed impaired memory compared to 5 \times FAD^{LV-GFP} mice (fig. S10).

Five-month-old 5 \times FAD mice in which AHN was ablated starting at 4 to 4.5 months of age performed comparably to 5 \times FAD^{CTL} mice in the RAM task (fig. S11). No impairment was observed in 3-month-old 5 \times FAD^{AHN} mice in which AHN was suppressed beginning at 1.5 to 2 months of age compared to those with AHN (fig. S12). These results suggest that loss of AHN, alone, is not sufficient to cause global hippocampal cognitive deficits in 5 \times FAD mice, and that loss of mature

granule neurons (owing to AHN loss at a much earlier age) is minimally required to result in global cognitive deficits later in life (beginning at 5 months of age).

Ablating AHN in male 5 \times FAD mice reduces hippocampal levels of TGF- β 1

The mechanisms by which the lack of AHN contributes to cell death in mature neural populations in 5 \times FAD mice are likely diverse with multiple pathways, and future efforts will be necessary to elucidate them. Among the cytokines we measured, transforming growth factor- β 1 (TGF- β 1) levels were significantly reduced in the hippocampal tissue homogenates of 5 \times FAD^{AHN (High KD)} mice compared to 5 \times FAD^{CTL} mice (Fig. 5A and table S5). TGF- β 1 levels were not reduced in WT^{AHN (High KD)} mice compared to WT^{CTL} mice (fig. S13), suggesting that AHN loss, accompanied by loss of granule cells and synaptic markers, results in the reduced TGF- β 1 levels. TGF- β 1 is an anti-inflammatory cytokine that increases rapidly after injury and with age (22). Neurons and multipotent NPCs produce TGF- β 1 (23, 24), and TGF- β 1 inhibits Casp3 (25). We asked whether TGF- β 1 has protective effects against cell death in AD, i.e., whether reduced TGF- β 1 levels in 5 \times FAD^{AHN} contribute to cell death. For this purpose, we increased TGF- β 1 in 5 \times FAD^{AHN} mice by injecting lentivirus expressing TGF- β 1 (LV-TGF- β 1; 5 \times FAD^{IR/LV-TGF- β 1}, 5 \times FAD^{TMZ/LV-TGF- β 1}, and 5 \times FAD^{LV-dnWnt/LV-TGF- β 1}) and quantified Casp3⁺ cells (Fig. 5, B to D). These mice experienced increased hippocampal TGF- β 1 levels and decreased numbers of Casp3⁺ cells in the DG compared to 5 \times FAD mice without AHN that were injected with control LV-RFP (5 \times FAD^{IR/LV-RFP}, 5 \times FAD^{TMZ/LV-RFP}, and 5 \times FAD^{LV-dnWnt/LV-RFP}). However, Casp3⁺ cells were still evident in the 5 \times FAD^{AHN} mice injected with LV-TGF- β 1, and increasing TGF- β 1 levels was not sufficient to rescue cell death fully in 5 \times FAD mice without AHN. Our results suggest that TGF- β 1 has protective effects against cell death in 5 \times FAD mice and that the reduced TGF- β 1 levels in 5 \times FAD mice without AHN, at least in part, contribute to granule cell death. Other mechanisms that maintain existing neuronal stability in AD likely account for the fraction of cell death that was not rescued by TGF- β 1. Increasing TGF- β 1 in 5 \times FAD^{AHN} mice did not change the degree of AHN (fig. S14), although TGF- β 1 has been shown to regulate neurogenesis (26–29).

Protective effects of TGF- β 1 against cell death were confirmed in three-dimensional (3D) cultures of differentiated human NPCs expressing familial AD-related mutations (3D-FAD cells) (30). Our 3D-FAD cells showed an increased number of Casp3⁺ cells and endogenous neuronal loss, as indicated by cell counting, compared to control WT cells (3D-WT cells) beginning at 5 weeks of differentiation (fig. S15). Six-week differentiated 3D-FAD cells were treated with TGF- β 1 for up to 2 weeks, after which cell viability was assessed. Casp3⁺ cell number was significantly reduced in 3D-FAD cells treated with TGF- β 1 (10 ng/ml; Fig. 5, E and F). Treatment of TGF- β 1 significantly

increased cell survival in 3D-FAD cells, as indicated by cell counting (Fig. 5, G and H). Furthermore, a lactate dehydrogenase (LDH) assay showed that treatment with TGF- β 1 resulted in decreased LDH release (fig. S16A). Protective effects of TGF- β 1 were also shown by a CellTiter-Glo luminescent assay, in which cell viability was increased with TGF- β 1 treatment (fig. S16B).

Endogenous levels of TGF- β 1 were measured in 0.5-, 5-, and 8-week differentiated 3D-WT and 3D-FAD cultures (fig. S17A). Considering that our 3D cultures are composed of mostly neurons, with astrocyte presence, and do not contain microglia, the endogenous TGF- β 1 detected in our 3D culture models was secreted from neurons and/or astrocytes. At 0.5 week of differentiation, TGF- β 1 levels were higher in the 3D-FAD cultures compared to 3D-WT. Whereas TGF- β 1 levels in the 3D-WT did not differ significantly at the three time points, in the 3D-FAD culture, levels of TGF- β 1 were significantly reduced in the 5- and 8-week differentiated cultures, where cell death occurred, compared to the 0.5-week differentiated cultures. When normalized by actin signal density, TGF- β 1 levels in the 5- and 8-week differentiated 3D-FAD cultures did not differ from those in age-matched 3D-WT cultures (fig. S17B), suggesting that the decrease in TGF- β 1 observed in 3D-FAD cultures compared to 3D-WT cultures was due to cell loss. However, we also observed that TGF- β 1 levels normalized by actin signal were significantly lower in the 8-week differentiated 3D-FAD cultures compared to 5-week-differentiated 3D-FAD cultures. Therefore, we cannot exclude the possibility that the reduced levels observed at the 8-week time point were also attributable to specific signaling inhibitions.

Effects of ablating AHN in female 5 \times FAD mice

AHN loss in female 5 \times FAD mice was accompanied by an increased number of Casp3⁺ cells in the DG, reduced hippocampal levels of PSD95, and exacerbated cognitive dysfunction (Fig. 6, A to E, and fig. S18; see fig. S18A for number of animals in each experimental group and group arrangement explanations). However, these mice did not show reduced hippocampal levels of TGF- β 1 (Fig. 6F). Thus, we measured endogenous levels of TGF- β 1 in the hippocampus of untreated male and female WT and 5 \times FAD mice at different ages (Fig. 6G). Untreated female 5 \times FAD mice showed significantly increased TGF- β 1 levels as compared to WT mice and increased, although not statistically significant, TGF- β 1 levels as compared to male 5 \times FAD mice at 5 months of age. The relatively increased levels of TGF- β 1 in female 5 \times FAD mice might mask the ability to observe a small reduction of TGF- β 1, as observed in male 5 \times FAD mice without AHN. Therefore, blocking AHN might result in reduction of TGF- β 1 in 5 \times FAD mice at an age when endogenous TGF- β 1 levels are not yet increased as compared to WT mice. AHN loss still increased Casp3⁺ cell numbers in female 5 \times FAD mice, suggesting that reduction of TGF- β 1 is most likely not the only mechanism underlying cell death in 5 \times FAD mice lacking AHN.

Exercise increased levels of hippocampal BDNF, PSD95, SYP, IL-6, and FNDC5

We addressed the mechanism by which the combination of exercise and increased AHN, but not increased AHN alone, improved cognition in the 5×FAD mice. Exercise has been shown to increase neurotrophins, growth factors, and synaptic markers and to reduce neuroinflammation (31–35). Exercise induces fibronectin type III domain-containing protein-5 (FNDC5) that regulates hippocampal BDNF expression in mice (36). We first measured 18 molecules in the hippocampus of untreated sedentary and exercised 5×FAD mice and found that exercise increased the levels of hippocampal BDNF, PSD95, synaptophysin (SYP), interleukin-6 (IL-6), and FNDC5 (table S6).

We next measured the levels of these molecules in the 5×FAD^{CTL}, 5×FAD^{ProAHN}, 5×FAD^{+AHN(RUN)}, and 5×FAD^{ψAHN(RUN)} mice. Exercise again led to increased levels of hippocampal BDNF, PSD95, SYP, IL-6, and only in male mice, FNDC5, whereas activating AHN alone did not (Table 1 and table S7). Considering that AD patients have reduced levels of BDNF, PSD95, and SYP (37–39) and that these proteins are important regulators of synaptic plasticity, the increase in these protein levels with exercise combined with increased AHN may contribute to an improved behavioral outcome for patients, as observed in the 5×FAD^{+AHN(RUN)} mice. IL-6, for which levels are selectively elevated in the hippocampus following exercise (40), has also been reported to benefit cognition and regulate neurogenesis (41–45).

AHN activation combined with increased BDNF levels genetically ameliorates cognitive function in 5×FAD mice

To explore the mechanisms underlying cognitive improvement after combined exercise and increased AHN, we directly increased BDNF, IL-6, or FNDC5 in the hippocampus of 5×FAD^{ProAHN} mice. We investigated whether increasing levels of these factors in conjunction with increased AHN would result in cognitive improvements mimicking those observed in the 5×FAD^{+AHN(RUN)} mice. To increase BDNF in the 5×FAD^{ProAHN} mice, lentivirus expressing BDNF (LV-BDNF) was injected into the hippocampus at 3 months of age when the mice received LV-Wnt3 (5×FAD^{ProAHN/LV-BDNF}; Fig. 7A). Lentivirus expressing red fluorescent protein (LV-RFP) was injected into additional 5×FAD^{ProAHN}

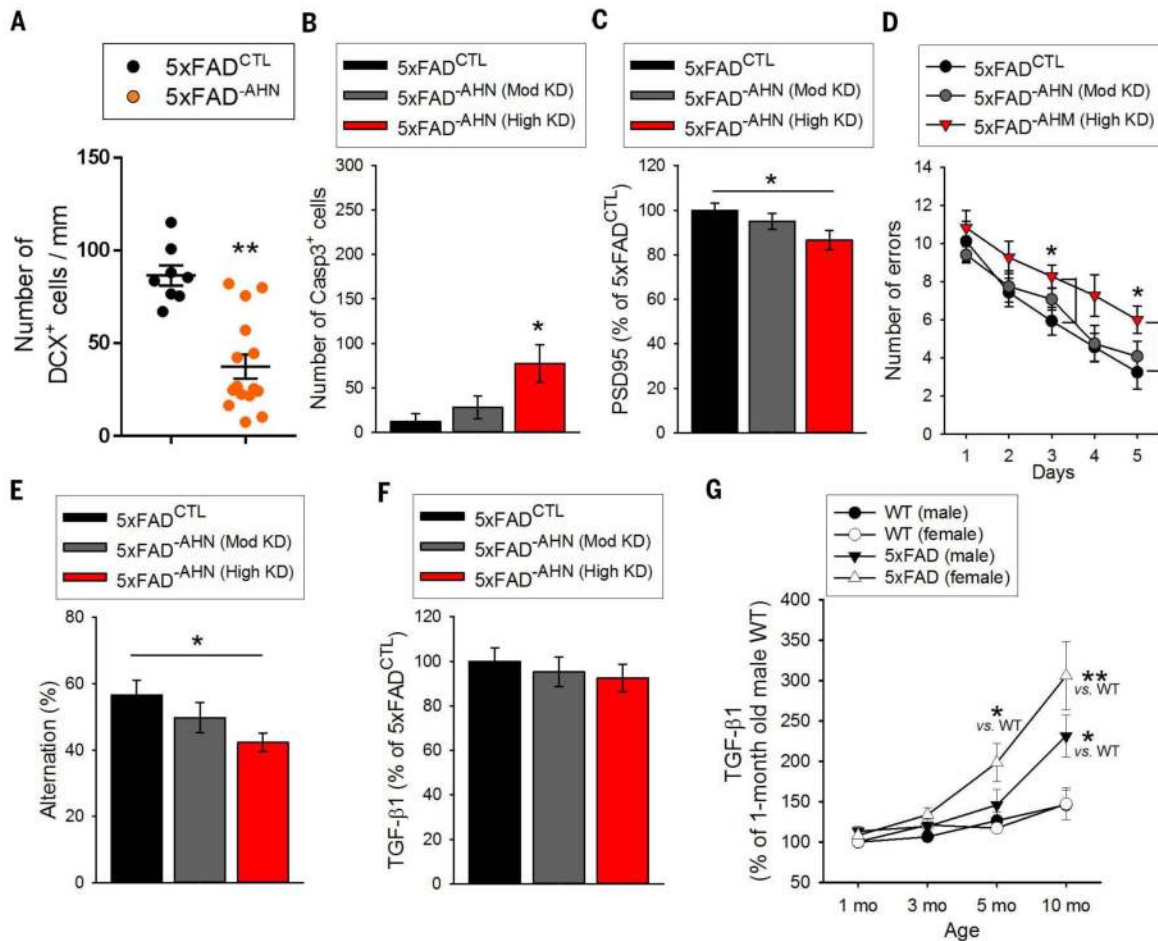


Fig. 6. Effects of ablating AHN in female 5×FAD mice. (A) Quantification of DCX⁺ cells in female 5×FAD^{CTL} and 5×FAD^{AHN} mice. (B) Quantification of Casp3⁺ cells in female 5×FAD^{CTL}, 5×FAD^{AHN (Mod KD)}, and 5×FAD^{AHN (High KD)} mice ($F_{(2,20)} = 4.803$, $P < 0.05$). (C) Levels of hippocampal PSD95 ($F_{(2,20)} = 3.499$, $P < 0.05$). Levels are shown as percent of 5×FAD^{CTL} group. (D) Mean error number in RAM task training trials. Two-way ANOVA with repeated measures revealed significant effects for days ($F_{(4,80)} = 24.19$, $P < 0.01$) and groups ($F_{(2,20)} = 5.982$, $P < 0.01$) but not interaction ($F_{(8,80)} = 0.4305$, $P = 0.8994$). Analysis of error number on each day by Fisher's LSD post hoc tests

revealed that 5×FAD^{AHN (High KD)} differed significantly from 5×FAD^{CTL} mice on days 3 and 5 (day 3, $F_{(2,20)} = 3.495$, $P < 0.05$; day 5, $F_{(2,20)} = 3.419$, $P = 0.0428$). (E) Spontaneous alternation in Y-maze ($F_{(2,20)} = 3.747$, $P < 0.05$). Total arm entries comparable among groups (fig. S18G). (F) Hippocampal TGF-β1 levels. Levels are shown as percent of 5×FAD^{CTL} group. (G) Changes in TGF-β1 levels in the hippocampal homogenates of untreated male and female WT and 5×FAD mice with age ($n = 7$ per group). In 5-month-olds, $*P < 0.05$ between female 5×FAD and WT mice. In 10-month-olds, $*P < 0.05$ between male 5×FAD and WT mice; $**P < 0.01$ between female 5×FAD and WT mice.

and 5×FAD^{+AHN(RUN)} mice (5×FAD^{ProAHN/LV-RFP} and 5×FAD^{+AHN(RUN)/LV-RFP} mice, respectively). LV-BDNF injection increased hippocampal BDNF levels in both 6-month-old male and female 5×FAD^{ProAHN} mice (Fig. 7B; see table S8 for statistical analysis of Fig. 7 experiments). Although BDNF has been shown to regulate AHN positively (46), LV-BDNF injection did not further increase the number of DCX⁺ neurons in 5×FAD mice treated with P7C3 and LV-Wnt3, and the number of DCX⁺ neurons was comparable in all groups (Fig. 7C). LV-BDNF injection did not affect Aβ plaque levels (Fig. 7D).

In the Y-maze, both male and female 5×FAD^{+AHN(RUN)/LV-RFP} mice showed improved memory compared to the 5×FAD^{ProAHN/LV-RFP} mice of both genders (Fig. 7E and fig. S19). 5×FAD^{ProAHN/LV-BDNF} mice also exhibited similar memory improvement. In male cohorts, during the RAM task training trials, 5×FAD^{+AHN(RUN)/LV-RFP} mice showed improved memory compared to 5×FAD^{ProAHN/LV-RFP} mice (Fig. 7F, left graph). Although 5×FAD^{ProAHN/LV-BDNF} mice did not show significant improvement, their performance did not differ from that of either 5×FAD^{ProAHN/LV-RFP} or 5×FAD^{+AHN(RUN)/LV-RFP} mice. However, in the memory retention test, 5×FAD^{ProAHN/LV-BDNF} mice showed memory improvement compared to 5×FAD^{ProAHN/LV-RFP} mice and behaved similarly to 5×FAD^{+AHN(RUN)/LV-RFP} mice (Fig. 7F, right graph). Increasing AHN alone by P7C3 and LV-Wnt3 did not improve pattern separation memory in female 5×FAD mice (Fig. 2A, right graph). However, increasing AHN in conjunction with BDNF in female 5×FAD mice (female 5×FAD^{ProAHN/LV-BDNF} mice) produced significantly improved pattern separation memory (Fig. 7G).

Increasing BDNF alone, in the absence of promoting AHN by P7C3 and LV-Wnt3, failed to increase AHN or improve memory in 5×FAD mice (Fig. 7, H and I, and fig. S20). These results suggest that increasing hippocampal BDNF, in combination with AHN activation, is sufficient to mimic the beneficial effects of exercise on cognition in 5×FAD mice, even in the continued presence of Aβ plaques.

AHN activation, combined with increased BDNF levels, pharmacologically ameliorates cognitive function in 5×FAD mice

We next explored whether a late-stage increase in BDNF pharmacologically (AICAR), with increased AHN by P7C3 and LV-Wnt3, could also provide an effective therapeutic strategy comparable to that of sustained exercise in 5×FAD mice. For this purpose, we used the AMP-activated protein kinase agonist 5-aminoimidazole-4-carboxamide riboside (AICAR), which increases BDNF in mice (47). Male and female 5×FAD^{ProAHN} mice were injected with AICAR or saline every other day for 2 weeks starting at 5.5 months of age; they were sacrificed at 6 months of age (5×FAD^{ProAHN/AICAR} and 5×FAD^{ProAHN/Veh} mice, respectively). Hippocampal BDNF levels were increased in the male and female 5×FAD^{ProAHN/AICAR} mice compared to 5×FAD^{ProAHN/Veh} mice, and their levels were not different from those of 5×FAD^{+AHN(RUN)} mice injected with saline (5×FAD^{+AHN(RUN)/Veh}; Fig. 7J). The number of DCX⁺ neurons was comparable among all groups (fig. S21A).

Male mice were tested in the Y-maze and RAM tasks, and female mice were tested in the Y-maze and DNMP tasks. In the Y-maze, 5×FAD^{ProAHN/AICAR} mice showed improved memory compared to the 5×FAD^{ProAHN/LV-RFP} mice in each respective gender, and their performance did not differ from that of 5×FAD^{+AHN(RUN)/Veh} mice (Fig. 7K and fig. S21B). Although male 5×FAD^{ProAHN/AICAR} mice did not perform better than 5×FAD^{ProAHN/Veh} mice in RAM task training trials (fig. S21C), they showed better cognition in the retention test of the task, performing similarly to 5×FAD^{+AHN(RUN)/Veh} mice (Fig. 7L). Female 5×FAD^{ProAHN/AICAR} mice showed improved pattern separation in the DNMP task, again performing similarly to 5×FAD^{+AHN(RUN)/Veh} mice (Fig. 7M).

It has been reported that AICAR alone increases AHN and cognition in WT mice (47, 48). However, AICAR alone failed to increase AHN in the 5×FAD mice, although it increased hippocampal BDNF levels (fig. S22A). No effect of

AICAR was observed in the cognition tasks that we employed in 5×FAD mice with no AHN activation (fig. S22B-S22D). These results suggest that a late-stage increase in BDNF by AICAR, in the presence of promoted AHN, could mimic the beneficial effects of exercise on cognition in 5×FAD mice.

Future studies will be needed to explore the mechanisms by which increasing levels of BDNF and AHN combine to mimic the benefits of exercise on cognition in AD. LV-BDNF injection increased levels of hippocampal PSD95, whereas AICAR did not (table S9). Neither LV-BDNF nor AICAR increased IL-6 levels (table S9). These results suggest that the beneficial effects of increasing both AHN and BDNF on cognition could be independent of PSD95 or IL-6. Directly increasing levels of hippocampal IL-6 or FNDC5 via lentivirus failed to improve cognition or increase BDNF in 5×FAD^{ProAHN} mice. However, it is possible that only the secreted form of peripherally expressed FNDC5 is responsible for exercise-induced hippocampal BDNF, as peripheral delivery of FNDC5 induces the expression of hippocampal BDNF (36). There may be other possible effects of AICAR aside from increasing BDNF levels. TGF-β1 levels were not changed by increasing AHN with or without increased BDNF, increasing BDNF only, or by exercise in our study (table S10).

Discussion

In the present study, we did not explore the effects of AHN manipulation on tau phosphorylation levels because basal tau phosphorylation is already present in adult-generated neurons at DCX⁺ immature neuronal stages [(49); see fig. S23]. Future studies are necessary to investigate whether adult-generated neurons affect tauopathy in the human AD brain. The effects of physical exercise on cognition in patients with dementia are inconclusive (50–52). In our study, 5×FAD^{+AHN(RUN)} mice did not show improved cognitive function, suggesting that increased AHN is required to mediate the beneficial effects of exercise in 5×FAD mice. Individuals who

Table 1. Levels of hippocampal BDNF, PSD95, SYP, IL-6, and FNDC5 of male 5×FAD^{CTL}, 5×FAD^{ProAHN}, 5×FAD^{+AHN(RUN)}, and 5×FAD^{+AHN(RUN)} mice. Animal numbers are in parentheses (results for female mice are in table S7). $F_{(3,31)} = 11.48$, $P < 0.01$ (BDNF); $F_{(3,41)} = 6.279$, $P < 0.01$ (PSD95); $F_{(3,41)} = 6.083$, $P < 0.01$ (SYP); $F_{(3,41)} = 6.047$, $P < 0.01$ (IL-6); $F_{(3,31)} = 5.974$, $P < 0.01$ (FNDC5). * $P < 0.05$; ** $P < 0.01$ compared to 5×FAD^{CTL} and 5×FAD^{ProAHN} mice.

| | 5×FAD ^{CTL} | 5×FAD ^{ProAHN} | 5×FAD ^{+AHN(RUN)} | 5×FAD ^{+AHN(RUN)} |
|-------|----------------------|-------------------------|----------------------------|----------------------------|
| BDNF | 100.00 ± 5.72 (8) | 91.32 ± 3.80 (10) | 149.74 ± 10.65** (8) | 145.29 ± 13.09** (9) |
| PSD95 | 100.00 ± 7.07 (10) | 103.19 ± 5.64 (15) | 129.39 ± 6.47* (12) | 128.23 ± 4.41* (8) |
| SYP | 100.00 ± 6.02 (10) | 102.03 ± 4.21 (15) | 125.59 ± 7.04* (12) | 125.02 ± 4.39* (8) |
| IL-6 | 100.00 ± 2.58 (10) | 105.44 ± 3.86 (15) | 128.89 ± 9.80* (12) | 129.52 ± 6.74* (8) |
| FNDC5 | 100.00 ± 6.54 (8) | 100.16 ± 7.49 (10) | 131.78 ± 6.26* (8) | 127.41 ± 7.03* (9) |

remain cognitively intact despite showing neuropathological AD features have increased numbers of neural stem cells compared to AD subjects (53). Therefore, future studies are required regarding whether patients with dementia who ex-

perienced physical exercise have increased AHN enough to have beneficial effects of exercise on cognition.

In summary, inducing AHN alone, e.g., pharmacologically and genetically, conferred only

minimal to no benefit in 5x*FAD* mice. However, exercise-induced AHN improved cognition along with reduced A β load and increased levels of BDNF, IL-6, FNDC5, and synaptic markers. AHN activation was also required for exercise-induced

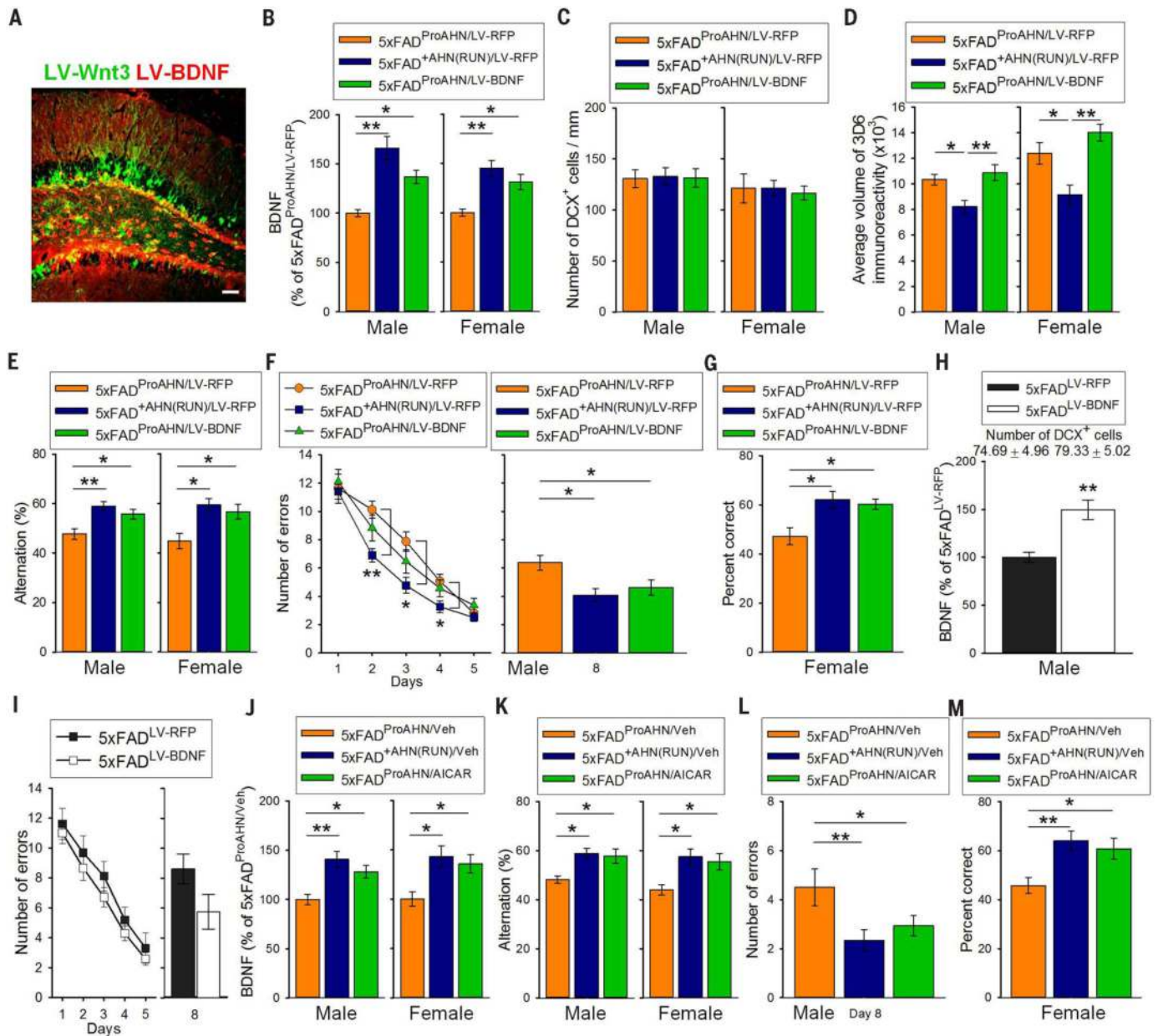


Fig. 7. AHN activation combined with increased BDNF levels ameliorates cognitive function in 5x*FAD* mice.

(A) Photomicrograph of lentiviral expression of LV-Wnt3 and LV-BDNF in the DG of 5x*FAD*^{ProAHN/LV-BDNF} mice. Scale bar: 50 μ m. (B) Hippocampal BDNF levels in 5x*FAD*^{ProAHN/LV-RFP}, 5x*FAD*^{+AHN(RUN)/LV-RFP}, and 5x*FAD*^{ProAHN/LV-BDNF} mice. (C) DCX⁺ cell quantification. (D) Quantitative analysis of A β burden volume (mean voxel count \pm SEM). (E) Spontaneous alternation behavior in Y-maze task. Total arm entries comparable among groups (fig. S19). (F) Left: mean error number for each group (male 5x*FAD*^{ProAHN/LV-RFP}, 5x*FAD*^{+AHN(RUN)/LV-RFP}, and 5x*FAD*^{ProAHN/LV-BDNF}) in RAM task training days. Right: mean error number in memory retention trial. (G) Quantification of percent correct during choice phase

of DNMP task among female 5x*FAD*^{ProAHN/LV-RFP}, 5x*FAD*^{+AHN(RUN)/LV-RFP}, and 5x*FAD*^{ProAHN/LV-BDNF} mice. (H) Hippocampal BDNF levels in male 5x*FAD*^{LV-RFP} ($n = 8$) and 5x*FAD*^{LV-BDNF} ($n = 12$) mice. DCX⁺ cell number per mm listed above graph. (I) Mean error number in RAM task training trials (left) and mean error number in memory retention trial (right). (J) Hippocampal BDNF levels in 5x*FAD*^{ProAHN/Veh}, 5x*FAD*^{+AHN(RUN)/Veh}, and 5x*FAD*^{ProAHN/AICAR} mice. (K) Spontaneous alternation behavior in Y-maze task. Total arm entries comparable among groups (fig. S21B). (L) Mean error number in memory retention trial of RAM task. (M) Quantification of percent correct during choice phase of DNMP task among female 5x*FAD*^{ProAHN/Veh}, 5x*FAD*^{+AHN(RUN)/Veh}, and 5x*FAD*^{ProAHN/AICAR} mice.

improvement in memory. These data suggest that promoting AHN can ameliorate AD pathology and cognitive deficits but only in the presence of a healthier, improved local brain environment, e.g., stimulated by physical exercise. Increasing AHN alone (genetically and pharmacologically) combined with overexpression of BDNF was able to mimic exercise-induced improvements in cognition, without reducing A β burden. We also found that deficits in AHN in very early stages of life can exacerbate neuronal vulnerability in AD later in life, leading to cognitive impairment and increased neuronal loss, due at least in part to reduced TGF- β 1. These results suggest that adult-born neurons generated very early in life are critical for maintaining hippocampal neuronal populations in the abnormal and hostile brain environment created by AD later in life. Thus, AHN impairment may be a primary event that later mediates other aspects of AD pathogenesis. Future attempts to create pharmacological mimetics of the benefits of exercise on both increased AHN and the health of the local neuronal environment, especially involving increased BDNF levels, may someday provide an effective means for improving cognition in AD. Moreover, increasing neurogenesis in the earliest stages of AD pathogenesis may protect against neuronal cell death later in the disease, providing a potentially powerful disease-modifying treatment strategy for AD.

Materials and Methods

Animals

We used 5 \times FAD APP/PS1 doubly transgenic mice that co-overexpress and co-inherit FAD mutant forms of human amyloid precursor protein (APP) (the Swedish mutation: K670N, M671L; the Florida mutation: I716V; the London mutation: V717I) and presenilin 1 (PS1) (M146L; L286V) transgenes under transcriptional control of the neuron-specific mouse Thy-1 promoter (Tg6799 line). 5 \times FAD lines (B6/SJL genetic background) were purchased from Jackson Laboratory and were maintained by crossing heterozygous transgenic mice with B6/SJL F1 breeders. All 5 \times FAD transgenic mice were heterozygotes with respect to the transgene. Animal experiments were conducted in accordance with institutional and NIH guidelines.

Observed benefits of employing the 5 \times FAD mouse model

Most of the current AD transgenic mouse models are generated by the overexpression of mutation (s) related to familial AD (FAD). While the 5 \times FAD mouse model expresses rare early-onset FAD mutations, the pathological features found in the brains of 5 \times FAD mice are common to all forms of AD. In the current study, we examined the manner in which altered AHN affects cell survival and cognition under these pathological conditions. Hence, we believe that the results of our experiments are also relevant for generalized AD pathology (beyond that of early-onset FAD).

We chose 5 \times FAD mice, which show faster AD progression compared to other AD transgenic

mice, based on our goal of investigating whether impaired AHN at an early stage in AD resulted in neuronal/synaptic loss and in accelerated cognitive impairment at later stages of the disease. We also aimed to investigate whether adult-generated neurons affected the pre-existing neuronal populations and whether impaired AHN exacerbated neuronal loss in AD.

5 \times FAD mice are one of the few AD transgenic mouse models that exhibit neurodegeneration, thus rationalizing our use of this model. In addition, performing long-term manipulations of AHN is challenging and can compromise the health of mice over time. For example, multiple irradiations cause neuro-inflammation. Long-term injections of TMZ cause side effects, including weight loss and hair loss (personal observations). Lentivirus is delivered to the brain using stereotaxic surgery, and multiple brain surgeries are not possible. Thus, studying the 5 \times FAD line, which undergoes more rapid AD progression compared to other AD transgenic mice, is advantageous for our study.

Generation of LV-Wnt3 and LV-dnWnt

To construct the Wnt3-Internal ribosomal entry site (IRES)-GFP vector, we cloned the cDNA of Wnt3 upstream of the IRES and GFP and inserted the bicistronic cassette in place of the GFP sequence in the pRRL.SIN.cPPT.hPGK.GFP.Wpre vector. To generate the dnWnt-IRES-GFP vector, we cloned the cDNA for dnWnt upstream of the IRES and GFP and inserted the bicistronic cassette in place of the GFP sequence in the CSC.cPPT.hCMV.GFP.Wpre vector. Concentrated lentiviral stocks were produced by calcium phosphate transfection into 293T cells. Supernatants were collected, passed through a 0.22- μ m filter, and purified by ultracentrifugation. Viral stocks were stored at -80°C until use and were diluted at 0.8×10^9 to 1×10^9 transducing units/ml.

Treatment of aminopropyl carbazole (P7C3) and LV-Wnt3, and exercise setting

To increase neurogenesis, 2-month-old 5 \times FAD mice received 20 mg/kg of P7C3 (Sigma, St. Louis, MO; Asinex, Winston-Salem, NC) once daily for 4 or 5 days a week intraperitoneally (i.p.) over the span of 4 to 4.5 months. P7C3 was prepared for dosing by dissolving a recrystallized stock in dimethyl sulfoxide (DMSO) at 50 mg/ml. The compound was diluted to a final formulation of 3% DMSO/10% cremophor EL (Sigma, St. Louis, MO)/87.5% D5W (5% dextrose in water, pH 7.2). At the age of 3 months, these mice also received 4 intrahippocampal injections of 0.5 μ l (total 2.0 μ l) LV-Wnt3 viral suspension at these coordinates: AP, -2.0 ; ML, ± 1.5 - 1.7 ; DV, -2.0 and AP, -3.0 ; ML, ± 3.0 ; DV, -3.0 . Injections were performed using a 5 μ l Hamilton syringe with a 30-gauge needle attached to a digital stereotaxic apparatus and an infusion pump at a rate of 0.15 μ l/min. After virus infusion was completed, the needle remained in place for 10 min before slow withdrawal. The mice were not injected with P7C3 both 3 days prior to and following the LV-Wnt3 injection day. Control 5 \times FAD mice received

vehicle solution [3% DMSO/10% cremophor EL (Sigma, St. Louis, MO)/87.5% D5W (5% dextrose in water, pH 7.2) with no P7C3] and LV-GFP.

Both groups were either singly housed either in standard laboratory cages (27 cm by 11 cm by 17 cm) only or singly spent 3 hours in rat cages (45 cm by 20 cm by 20 cm) without running wheels and then were returned to their original cages for 21 hours. A cohort of control 5 \times FAD mice treated with vehicle and LV-GFP singly spent 3 hours in rat cages equipped with running wheels and was returned to their original cages for the remaining 21 hours, as described previously (17), from between the ages of 6 weeks and 2 months until the end of the experiments.

To evaluate potential changes in neurogenesis, we determined the number of DCX $^{+}$ cells in the targeted (GFP-expressing) areas. Areas infected by LVs were identified by expression of GFP.

Blocking AHN

To block AHN, 1.5- to 2-month-old WT and 5 \times FAD mice received IR, TMZ or LV-dnWnt and were sacrificed at 3 or 5 months of age. Irradiation was not used for mice that were sacrificed at 3 months of age because it requires ~ 1 month of recovery time. Additional 4- to 4.5-month-old 5 \times FAD mice received TMZ or LV-dnWnt and were sacrificed at 5 months of age.

Irradiation procedure

Mice were anesthetized with ketamine and xylazine, placed in a stereotaxic frame, and put into a custom-made radiation shield consisting of a chamber with 1-inch-thick lead and a 2.5-mm borehole. The shield covered the entire body but left a 2.5-mm treatment field above the hippocampus. Mice received irradiation once at the dose of 1000 cGy, administered at ~ 90 cGy per minute for a total irradiation time of 11 min. A Gammacell 40 Exactor (Theratronics, Ottawa, Ontario) with two cesium-139 sources was used.

TMZ injection

The DNA-alkylating agent TMZ (Merck & Co., Inc., Whitehouse Station, NJ; Sigma, St. Louis, MO) was dissolved in phosphate-buffered saline (PBS) or in DMSO followed by diluting in PBS to a concentration of 2.5 mg/ml (10% DMSO for TMZ from Sigma). TMZ was administered i.p. at a dose of 12.5 mg/kg once daily for 3 consecutive days, followed by 4 days of no injections (one cycle). After every four cycles, mice were given a 2-week rest period. Vehicle solution was the identical DMSO/PBS solution but without TMZ and was administered in volumes consistent with TMZ dosing.

LV-dnWnt injection

Stereotaxic injections of LV-dnWnt were performed as described above for LV-Wnt3 injections.

Injections of LV-TGF- β 1 and LV-BDNF

LV-TGF- β 1, LV-BDNF, LV-IL-6, IL-FNDC5, and control LV-RFP were purchased from ViGene Biosciences (Rockville, MD). 5 \times FAD^{Sham}, 5 \times FAD^{IR}, 5 \times FAD^{Veh}, and 5 \times FAD^{TMZ} mice received four

intra-hippocampal injections of 0.5 μ l (total 2.0 μ l) of LV-TGF- β 1 or LV-RFP viral suspension (AP, -2.0; ML, \pm 1.5 to 1.7; DV, -2.0 and AP, -3.0; ML, \pm 3.0; DV, -3.0) at the age of 2.5 to 3 months. For injections of LV-dnWnt along with LV-TGF- β 1 or LV-RFP in 5 \times FAD mice, 1.5- to 2-month-old mice received four intra-hippocampal injections of total 2.4 to 3.0 μ l of LV-dnWnt with LV-TGF- β 1 or LV-RFP viral suspension. For injection of LV-BDNF, 5 \times FAD^{ProAHN} mice received LV-BDNF at the age of 3 months when they received LV-Wnt3: total 2.4 to 3.0 μ l of LV-Wnt3 with LV-BDNF or LV-RFP viral suspension.

Treatment of 5-aminoimidazole-4-carboxamide-1- β -D-ribofuranoside (AICAR)

Mice were injected (i.p.) with AICAR (Toronto Research Chemicals Inc., Canada) dissolved in saline, 250 mg/kg per day, or with saline, every other day for 2 weeks. During the 2 weeks, P7C3 was not injected.

5-Bromo-2'-deoxyuridine (BrdU) injections

BrdU (Sigma, St. Louis, MO) was dissolved in 0.9% NaCl at a concentration of 20 mg/ml and was filtered (0.2 μ m) under sterile conditions. Mice received a single i.p. injection of BrdU (50 mg/kg) daily for 3 days and were perfused 1 day after the last BrdU injection and processed for BrdU immunostaining to identify proliferating neural progenitor cells (NPCs). Parallel cohorts of animals from each group were sacrificed 4 weeks after the last BrdU injection and processed to determine the rate of NPC survival and differentiation.

Behavior tests

We performed three different behavioral tests: a delayed nonmatching to place (DNMP) task to measure pattern separation, an eight-arm radial arm maze (RAM) to measure reference memory and retention memory, and a Y-maze to measure short-term spatial (working) memory. For the DNMP and RAM tasks, mice were food restricted to 90% of their pre-experimental free-feeding weights with water available ad libitum. We confirmed that our food deprivation regime did not affect AHN in WT and 5 \times FAD mice. Behavior analyses were performed blindly.

DNMP task

Pattern separation-dependent memory was tested in the DNMP task in the RAM apparatus as described previously (16) with modifications. The testing apparatus was a rat-sized RAM. The maze consisted of eight equally spaced arms that radiated from an octagonal central platform. Arms were 15 cm wide by 75 cm long, and the walls on each arm were 2.5 cm high. On the morning before testing commenced, mice were habituated to the maze, where all arms were unblocked and all wells at the end of the arms contained several sunflower seeds. Mice were allowed to explore the maze freely during this habituation session for 30 min. Each trial of this task consisted of a sample phase and a choice phase.

During the sample phase, all arms except a start arm and the sample (rewarded) arm were blocked off. Each mouse was permitted to visit the sample arm and retrieve a food pellet reward. Mice were retrieved from the maze after either (1) spending 10 s in the sample arm after retrieving the pellet or (2) exiting the sample arm. During the choice phase, arms in the start and sample (unrewarded) locations and an additional correct (rewarded) location were open. The correct arm was distant from the sample arm by a spatial separation of two arms. In this phase, mice were tested for the ability to select, from a choice of two arms, the arm location that had not been presented in a previous sample phase. Mice that entered the correct (new, rewarded) arm were considered to have made correct choices. Mice that entered an incorrect (familiar, unrewarded) arm were allowed to self-correct. Mice went through four trials (sample plus choice phases) per day for 3 consecutive days.

RAM

The RAM was used for testing spatial reference and retention memory. To adapt to the maze and bait (pretraining), the mice experienced free movement and feeding in a RAM twice a day for 2 days. The bait was scattered in all arms and a sunflower seed in a food cup was available at the end of each arm. The training trial was started following the pretraining. During the training trial, each mouse was given two trials daily for 5 days. The same two arms were baited each day and across sessions; thus mice learned to ignore the remaining six arms that never contained a reward. A trial consisted of placing the mouse in the maze where it remained until both of the two reinforcements had been received or until 5 min had elapsed, whichever occurred first. Entry into a never-baited arm was considered a reference memory error, and choices of arms were recorded. Memory retention trial was conducted 3 days after the last training trial in the reference memory test of RAM task.

Y-maze

Short-term spatial memory was assessed by recording spontaneous alternation behavior in a Y-maze, which does not involve any training, reward, or punishment. The ability to alternate requires mice to know which arms have already been visited. Therefore, alternation behavior can be regarded as a measure involving spatial working memory. Each mouse was placed in the center of the symmetrical Y-maze and was allowed to explore freely through the maze during an 8-min session. The sequence and total number of arms entered were recorded. Arm entry was considered to be complete when the hind paws of the mouse had been completely placed in the arm. An alternation was defined as entries into all three arms on consecutive occasions. The number of maximum alternation was therefore the total number of arm entries minus 2, and the percentage of alternation was calculated as (actual alternations / maximum alternations) \times 100.

Tissue processing

After behavioral tasks, mice were deeply anesthetized with a mixture of ketamine and xylazine and then decapitated. Isolated brains were bisected longitudinally and hemispheres were separated. Hippocampal tissues were dissected from the left hemisphere and frozen on dry ice for biochemical studies. The right hemisphere was kept in 4% paraformaldehyde (PFA) in cold 0.1 M phosphate buffer (pH 7.4) for 3 days, followed by incubation in 30% sucrose solution for immunostaining. Mice injected with BrdU were deeply anesthetized with a mixture of ketamine and xylazine, and perfused transcardially with 4% PFA in cold 0.1 M phosphate buffer (pH 7.4) after 0.9% NaCl. The brains were postfixed overnight and then transferred into a 30% sucrose solution and kept there until they sank. For immunostaining, 40- μ m coronal sections were cut from a dry ice-cooled block on a sliding microtome (Leica, Wetzlar, Germany). The sections were stored at -20°C in a cryoprotective buffer containing 28% ethylene glycol, 23% glycol, and 0.05 M phosphate buffer until processing for immunohistochemistry or immunofluorescence.

Immunohistochemistry and immunofluorescence confocal microscopy

Immunohistochemistry and immunofluorescent labeling were performed as described previously (54). The antibodies used were rat anti-BrdU (1:100, Accurate Chemical & Scientific Corporation, Westbury, NY), biotin-conjugated mouse anti-BrdU (1:100, Millipore, Temecula, CA), goat anti-DCX (1:200, Santa Cruz Biotechnology, Dallas, Texas), mouse anti-neuronal nuclei (NeuN, 1:500, Chemicon, Temecula, CA), rabbit anti-Fox3/NeuN (1:500, EnCor Biotechnology Inc., Gainesville, FL), rabbit anti-Glial Fibrillary Acidic Protein (GFAP, 1:500, Dako, Fort Collins, CO), rabbit anti-ionized calcium-binding adaptor molecule 1 (Iba1, 1:500, Wako, Osaka, Japan), goat anti-Iba1 (1:500, Abcam, Cambridge, MA), mouse anti-A β 3D6 antibodies (1:2,500, a gift from Lilly), and rabbit monoclonal anti-cleaved Caspase 3 (Casp3, 1:1,000, Cell signaling, Danvers, MA).

The immunohistochemical staining was made using the avidin-biotin complex (ABC) system and nickel-enhanced diaminobenzidine (DAB) incubation (Vectastain Elite, Vector labs, Burlingame, CA). Sections were mounted on gelatin-coated slides, air-dried, dehydrated, cleared, and coverslipped. The fluorescent secondary antibodies used for immunofluorescent labeling were donkey anti-goat immunoglobulin G (IgG) conjugated with Cy2 or Cy3; donkey anti-rat IgG conjugated with Cy2 or Cy3; donkey anti-mouse IgG conjugated with Cy2 or Cy3 or Cy5; donkey anti-rabbit IgG conjugated with Cy2 or Cy3 or Cy5 (all 1:250, Jackson ImmunoResearch, West Grove, PA). Fluorescent signals were detected using a LSM Pascal 5 Carl Zeiss confocal laser scanning microscope (Zeiss, Germany). Images were captured and recorded using a Zeiss LSM image browser.

For BrdU staining, DNA was denatured by incubating the sections for 2 hours in the 50%

formamide/2× SSC (0.3 M NaCl and 0.03 M sodium citrate) at 65°C. Sections were rinsed for 15 min in 2× SSC and incubated for 30 min in 2 N HCl at 37°C. Acid was neutralized by rinsing the sections for 10 min in 0.1 M boric acid (pH 8.5) followed by several washes in Tris-buffered saline (TBS, pH 7.5).

Quantification of immunoreactivity and mouse regrouping

For estimating total BrdU⁺ cells, a series of systematically selected every sixth brain section was stained, and BrdU⁺ cells in the subgranular cell layer (SGL) and granular cell layer (GCL) were counted by collecting images under 40× objective on a light microscope (TE360 Eclipse, Nikon, Japan) or a confocal microscope (LSM Pascal 5 Carl Zeiss, Germany). The sum of the BrdU⁺ cell counts was multiplied by 6 to obtain an estimate of total numbers. For co-labeling analysis of differentiated BrdU⁺ cell types with lineage-specific markers, the phenotypes of 30 BrdU⁺ cells per animal were determined. Both the BrdU⁺ cell count and the phenotype analysis were performed blindly.

For quantification of DCX⁺ cells, a series of systematically selected every 6th or 12th brain section from each mouse was taken from similar regions spanning between bregma −1.34 mm and −3.28 mm using a Mouse Brain Atlas [Paxinos G, Franklin KBJ (2001) The mouse brain in stereotaxic coordinates, Academic Press, San Diego]. The numbers of DCX⁺ cells were counted in the inner rim, defined as the border between the hilus and GCL, under 20× objective lens manually. The inner rim length of GCL was measured using a Zeiss LSM image browser (Carl Zeiss, Germany) or Imaris software (Bitplane, Concord, MA). Based on the results of DCX⁺ cell numbers, mice were regrouped for additional behavioral data analysis and biochemical/immunostaining experiments. See tables S1 and S2, and fig. S18A for the number of animals in each experimental group and explanations of group arrangement.

For quantification of Casp3⁺ cells, a series of systematically selected every sixth brain section was stained, and Casp3⁺ cells in the SGL and GCL were counted by collecting images under 40× objective on a light microscope (TE360 Eclipse, Nikon, Japan) or a confocal microscope (LSM Pascal 5 Carl Zeiss, Germany). The sum of the Casp3⁺ cell counts was multiplied by 6 to obtain an estimate of total numbers. Researchers who were unaware of the experimental group to which the samples belonged quantified DCX⁺ or Casp3⁺ cells.

Total granule cell counting

Granule cell numbers were determined using unbiased stereologic counting methods. Each sixth section containing the hippocampus was Nissl stained. Optical disector frames (15 × 15 μm) were set in as systematic-random fashion, accounting for 1% of the area of the GCL on each section. Cells were counted in 5-μm-thick stacks of optical disectors (1 μm in depth for each di-

sector), according to stereologic principles. The total number of GCL neurons was obtained by using the formula developed as described previously (55). The granule cell counting was performed blindly.

Quantitative assessment of amyloid deposition

To examine the impact of AHN manipulation or exercise on amyloid deposition, a series of systematically selected (every 12th) brain sections from each mouse was probed with Aβ-specific 3D6 antibodies, detected by fluorescently labeled secondary antibodies. Images to quantify the amyloid burden were collected in a Z series of 40-μm depth with 4-μm intervals between images. The volume of amyloid burden was quantified using ImageJ (Voxel counter plugin), and the area of Aβ immunoreactivity was assessed after adequate thresholding and isolated noise despeckling.

Quantitative cytokine level measurement and ELISAs

Hippocampal tissues were homogenized in RIPA buffer (Sigma, St. Louis, MO) and centrifuged at 45,000g for 30 min at 4°C. Supernatants were used to measure 10 cytokines: Interleukin 1β (IL-1β), IL-2, IL-4, IL-5, IL-6, IL-10, IL-12p70, tumor necrosis factor α (TNFα), interferon-γ (IFN-γ), and keratinocyte-derived chemokine (KC/GRO). The measurement of cytokines was performed using the MesoScale Discovery (MSD, Rockville, MD) 96-well Mouse Pro-Inflammatory V-PLEX Assay as outlined in the manufacturer's protocol. Briefly, 25 μl each of sample and calibrator were added to the plate coated with an array of cytokine capture antibodies. The plate was then incubated for 2 hours with vigorous shaking at room temperature, followed by washing with wash buffer (provided in the kit). A volume of 25 μl of the detection antibody solution was added and incubated for 2 hours with vigorous shaking at room temperature. The plate was washed with wash buffer before adding 150 μl 2× MSD Read Buffer, and immediately read on a Meso QuickPlex SQ 120.

For TGF-β1, PSD95, SAP97, SYP, and FNDC5 analyses, supernatant samples were further diluted in cold PBS. For TGF-β1, diluted samples were acidified to pH < 3 with 1 N HCl and incubated for 1 hour at room temperature, followed by neutralization to pH ~8 with 1 N NaOH. Levels of TGF-β1 were measured using TGF-β1 Platinum ELISA kits (Affymetrix eBioscience, San Diego, CA) according to the manufacturer's protocols. PSD95, SAP97, SYP, and FNDC5 contents were measured using ELISA kits from MyBioSource (San Diego, CA) according to the manufacturer's protocols. BDNF protein levels were measured using BDNF ELISA kits (R&D Systems, Minneapolis, MN). TGF-β1 in the media of the 3D cultures were measured using the MSD 96-well TGF-β1 kit (Rockville, MD).

Immunoblot analysis

Fifteen to 75 μg of protein were resolved on 12% Bis-Tris or 4 to 12% gradient Bis/Tris gels (Life

Technologies, Grand Island, NY), and the proteins were transferred to the nylon membranes (Bio-Rad, Hercules, CA). Immunoblot images were visualized by enhanced chemiluminescence (ECL). The images were captured by using BioMax film (Kodak, Rochester, NY) or VersaDoc imaging system (Bio-Rad, Hercules, CA) and quantitated by using QuantityOne software (Bio-Rad, Hercules, CA). Primary antibodies were used at the following dilutions: anti-PSD95 (1:500, NeuroMab, Davis, CA), anti-synapse-associated protein 97 (SAP97, 1:500, NeuroMab, Davis, CA), and anti-synaptophysin (SYP, 1:1,000, Millipore, Temecula, CA).

Golgi staining

Golgi staining was performed using the FD Rapid Golgi Stain Kit (FD Neurotechnologies, Inc., Columbia, MD), a simplified and reliable kit for Golgi impregnation, to label neurons in the outer layer of GCLs. Animals were deeply anesthetized with an isoflurane, and the brains were immediately removed and rinsed in MilliQ water. After the rinse, retrieved brains were immersed in a Golgi-Cox solution comprising potassium dichromate, mercuric chloride, and potassium chromate. This mixture of solutions was replaced once after 6 hours of initial immersion, with storage at room temperature in darkness for 2 weeks. After the immersion period in the Golgi-Cox solution, the embedded brains were transferred to a cryoprotectant solution (FD Rapid Golgi Stain Kit) and stored at room temperature for at least 72 hours in the dark before cutting. The brain slices were sectioned in the coronal or sagittal plane at approximately 250 μm thickness on a cryostat. Sliced tissues were transferred onto gelatin-coated slides and were air dried at room temperature in the dark. After drying, sections were rinsed with distilled water and were subsequently stained in a developing solution (FD Rapid Golgi Stain Kit) and dehydrated with 50, 75, 95, and 100% ethanol. Finally, the sections were defatted in xylene substitute and coverslipped with either Permount (Fisher Scientific, Fair Lawn, NJ).

Images were acquired from prepared slides using a Zeiss 510 microscope. Each neuron was scanned under high (100×, oil immersion) magnification by varying the depth of the Z plane to ensure that all parts of the cell (especially dendrites) were intact. Dendrites that tapered to a point were assumed to be complete and uncut. At least 20 neurons were selected. 3D neuronal reconstruction was performed by LSM510 (Zeiss). The total length and number of branches of dendrites and the spine density were measured by Imaris software (Bitplane, Concord, MA). Seven neurons per mouse were examined.

Treatment of 3D FAD ReN cell cultures with TGF-β1

ReNcell VM human NPCs (ReN cells, EMD Millipore, Billerica, MA) were transfected with internal ribosome entry site (IRES)-mediated polycistronic lentiviral vectors containing FAD genes encoding human APP with both Swedish (K670N/M671L) and London (V717I) mutations, or PS1ΔE9

mutation along with APP Swedish/London mutations, with GFP as a reporter for viral infection. Fluorescence-activated cell sorting (FACS) was then used to enrich the population of cells with the highest expression levels. ReN cells with GFP alone served as controls. The FACS-sorted ReN cells expressing high levels of FAD genes were differentiated and maintained in a 3D Matrigel culture system. Differentiation media containing either 1, 5, or 10 ng/ml of active human TGF- β 1 (Abcam, Cambridge, MA) were added to 6-week differentiated cultures every 3 days, and the cells were maintained for an additional 2 weeks. The cell media were collected for Lactate dehydrogenase (LDH) assay, CellTiter-Glo luminescent cell viability assay and A β quantification. The cells were fixed with 4% PFA for Casp3 staining.

LDH assay

CytoTox-ONE assay was performed according to the manufacturer's guidelines (Promega, Madison, WI). Fifty microliters of cell culture medium was removed from the cells and substrate was added to the cell culture medium in 1:1 dilution and incubated for 30 min in a 37°C incubator. The plate was measured using a spectrophotometer (excitation: 560 nm, emission: 590 nm). Under the influence of the assay's substrate, resazurin is converted to the fluorescent form resorufin due to LDH, which is released into the medium by dead cells only. Therefore, increased values during the experiments were interpreted as increased cell death.

CellTiter-Glo luminescent cell viability assay

Cell viability was determined using the CellTiter-Glo luminescent cell viability kit from Promega Corporation (Madison, WI) according to the manufacturer's instructions. This method was based on the measurement of ATP production in the cells, which is proportional to the number of viable cells, detected by luciferin-luciferase reaction. One hundred microliters of CellTiter-Glo Reagent was added into the wells. Contents were mixed for 2 min on an orbital shaker to induce cell lysis. The plate was allowed to incubate at room temperature for 10 min to stabilize luminescent signal, and luminescence was recorded.

Casp3 staining using 3D cultures

The fixed cells were permeabilized and blocked by incubating with a blocking solution containing 50 mM Tris (pH 7.4), 0.1% Tween-20, 4% donkey serum, 1% BSA, 0.1% gelatin, and 0.3 M glycine at 4°C for 12 hours. After washing with TBS buffer containing 0.1% (v/v) Tween-20 (TBST), the 3D cultures were incubated with rabbit monoclonal anti-cleaved Casp3 (1:1,000, Cell signaling, Danvers, MA) antibodies in the blocking solution at 4°C overnight. After washing three times with TBST, the cells were incubated with donkey anti-rabbit IgG conjugated Cy3 for 2 hours at room temperature (1:250, Jackson Immuno-Research, West Grove, PA). To avoid fluorescence quenching, a drop of anti-fade gold (Life Technologies, Grand Island, NY) was added on top of

the fixed/stained thin-layer 3D cultures before imaging.

Dot-blot analysis

3D Matrigel samples were dissolved in Lysis Buffer 6 (R&D Systems, Minneapolis, MN) with protease and phosphatase inhibitors (Thermo Scientific, Rockford, IL). One microliter of each sample was spotted onto a LI-COR Biosciences Odyssey Nitrocellulose Membrane (LI-COR Biosciences, Lincoln, NE). The dot blot was then stained for Monoclonal Anti- β -Actin-Peroxidase antibody produced in mouse (Sigma Aldrich, St. Louis, MO) overnight at a dilution ratio of 1:50,000. Then, after sufficient washing the following day, the blot was coated with 2 ml of Pierce ECL Western Blotting Substrate (Thermo Scientific, Rockford, IL). Chemiluminescent detection imaging was then conducted using the Chemi exposure setting on a Li-Cor Odyssey FC machine (LI-COR Biosciences, Lincoln, NE) and then quantified using Image Studio software (LI-COR Biosciences, Lincoln, NE).

Statistical analysis

Data are expressed as mean values \pm standard error of the mean (mean \pm SEM). Error bars in the figures represent SEM. Differences between groups were analyzed using a *t*-test or an ANOVA that was followed by a post hoc comparison using Tukey or Fisher's least significant difference (LSD), where appropriate. For the RAM tests, a two-way repeated measures analysis of ANOVA was used for main effects (groups) with day as the repeated measure and errors as the dependent variable. In all cases, values of $P < 0.05$ were considered to be significant, and * or # indicated $P < 0.05$ and ** or ## indicated $P < 0.01$. Statistical analysis was performed using PRISM GraphPad statistical software.

REFERENCES AND NOTES

- R. E. Tanzi, L. Bertram, Twenty years of the Alzheimer's disease amyloid hypothesis: A genetic perspective. *Cell* **120**, 545–555 (2005). doi: [10.1016/j.cell.2005.02.008](https://doi.org/10.1016/j.cell.2005.02.008); pmid: [15734686](https://pubmed.ncbi.nlm.nih.gov/15734686/)
- P. S. Eriksson *et al.*, Neurogenesis in the adult human hippocampus. *Nat. Med.* **4**, 1313–1317 (1998). doi: [10.1038/3305](https://doi.org/10.1038/3305); pmid: [9809557](https://pubmed.ncbi.nlm.nih.gov/9809557/)
- Y. Mu, F. H. Gage, Adult hippocampal neurogenesis and its role in Alzheimer's disease. *Mol. Neurodegener.* **6**, 85–93 (2011). doi: [10.1186/1750-1326-6-85](https://doi.org/10.1186/1750-1326-6-85); pmid: [22192775](https://pubmed.ncbi.nlm.nih.gov/22192775/)
- L. Crews *et al.*, Increased BMP6 levels in the brains of Alzheimer's disease patients and APP transgenic mice are accompanied by impaired neurogenesis. *J. Neurosci.* **30**, 12252–12262 (2010). doi: [10.1523/JNEUROSCI.1305-10.2010](https://doi.org/10.1523/JNEUROSCI.1305-10.2010); pmid: [20844121](https://pubmed.ncbi.nlm.nih.gov/20844121/)
- D. Gomez-Nicola *et al.*, Temporal dynamics of hippocampal neurogenesis in chronic neurodegeneration. *Brain* **137**, 2312–2328 (2014). doi: [10.1093/brain/awu155](https://doi.org/10.1093/brain/awu155); pmid: [24941947](https://pubmed.ncbi.nlm.nih.gov/24941947/)
- K. Jin *et al.*, Increased hippocampal neurogenesis in Alzheimer's disease. *Proc. Natl. Acad. Sci. U.S.A.* **101**, 343–347 (2004). doi: [10.1073/pnas.2634794100](https://doi.org/10.1073/pnas.2634794100); pmid: [14660786](https://pubmed.ncbi.nlm.nih.gov/14660786/)
- B. Li *et al.*, Failure of neuronal maturation in Alzheimer disease dentate gyrus. *J. Neuropathol. Exp. Neurol.* **67**, 78–84 (2008). doi: [10.1097/nen.0b013e318160c5db](https://doi.org/10.1097/nen.0b013e318160c5db); pmid: [18091557](https://pubmed.ncbi.nlm.nih.gov/18091557/)
- M. A. Lovell, H. Geiger, G. E. Van Zant, B. C. Lynn, W. R. Markesbery, Isolation of neural precursor cells from Alzheimer's disease and aged control postmortem brain. *Neurobiol. Aging* **27**, 909–917 (2006). doi: [10.1016/j.neurobiolaging.2005.05.004](https://doi.org/10.1016/j.neurobiolaging.2005.05.004); pmid: [15979211](https://pubmed.ncbi.nlm.nih.gov/15979211/)

- E. K. Perry *et al.*, Neurogenic abnormalities in Alzheimer's disease differ between stages of neurogenesis and are partly related to cholinergic pathology. *Neurobiol. Dis.* **47**, 155–162 (2012). doi: [10.1016/j.nbd.2012.03.033](https://doi.org/10.1016/j.nbd.2012.03.033); pmid: [22504537](https://pubmed.ncbi.nlm.nih.gov/22504537/)
- H. Oakley *et al.*, Intraneuronal beta-amyloid aggregates, neurodegeneration, and neuron loss in transgenic mice with five familial Alzheimer's disease mutations: Potential factors in amyloid plaque formation. *J. Neurosci.* **26**, 10129–10140 (2006). doi: [10.1523/JNEUROSCI.1202-06.2006](https://doi.org/10.1523/JNEUROSCI.1202-06.2006); pmid: [17021169](https://pubmed.ncbi.nlm.nih.gov/17021169/)
- O. Lazarov *et al.*, Environmental enrichment reduces Abeta levels and amyloid deposition in transgenic mice. *Cell* **120**, 701–713 (2005). doi: [10.1016/j.cell.2005.01.015](https://doi.org/10.1016/j.cell.2005.01.015); pmid: [15766532](https://pubmed.ncbi.nlm.nih.gov/15766532/)
- Z. Radak *et al.*, Exercise plays a preventive role against Alzheimer's disease. *J. Alzheimers Dis.* **20**, 777–783 (2010). doi: [10.3233/JAD-2010-091531](https://doi.org/10.3233/JAD-2010-091531); pmid: [20182027](https://pubmed.ncbi.nlm.nih.gov/20182027/)
- H. van Praag, G. Kempermann, F. H. Gage, Running increases cell proliferation and neurogenesis in the adult mouse dentate gyrus. *Nat. Neurosci.* **2**, 266–270 (1999). doi: [10.1038/6368](https://doi.org/10.1038/6368); pmid: [10195220](https://pubmed.ncbi.nlm.nih.gov/10195220/)
- A. A. Pieper *et al.*, Discovery of a proneurogenic, neuroprotective chemical. *Cell* **142**, 39–51 (2010). doi: [10.1016/j.cell.2010.06.018](https://doi.org/10.1016/j.cell.2010.06.018); pmid: [20603013](https://pubmed.ncbi.nlm.nih.gov/20603013/)
- D. C. Lie *et al.*, Wnt signalling regulates adult hippocampal neurogenesis. *Nature* **437**, 1370–1375 (2005). doi: [10.1038/nature04108](https://doi.org/10.1038/nature04108); pmid: [16251967](https://pubmed.ncbi.nlm.nih.gov/16251967/)
- C. D. Clelland *et al.*, A functional role for adult hippocampal neurogenesis in spatial pattern separation. *Science* **325**, 210–213 (2009). doi: [10.1126/science.1173215](https://doi.org/10.1126/science.1173215); pmid: [19590004](https://pubmed.ncbi.nlm.nih.gov/19590004/)
- L. Deuker, C. F. Doeller, J. Fell, N. Axmacher, Human neuroimaging studies on the hippocampal CA3 region - integrating evidence for pattern separation and completion. *Front. Cell. Neurosci.* **8**, 64 (2014). doi: [10.3389/fncel.2014.00064](https://doi.org/10.3389/fncel.2014.00064); pmid: [24624058](https://pubmed.ncbi.nlm.nih.gov/24624058/)
- J. Götz, L. M. Ittner, Animal models of Alzheimer's disease and frontotemporal dementia. *Nat. Rev. Neurosci.* **9**, 532–544 (2008). doi: [10.1038/nrn2420](https://doi.org/10.1038/nrn2420); pmid: [18568014](https://pubmed.ncbi.nlm.nih.gov/18568014/)
- D. Meshi *et al.*, Hippocampal neurogenesis is not required for behavioral effects of environmental enrichment. *Nat. Neurosci.* **9**, 729–731 (2006). doi: [10.1038/nn1696](https://doi.org/10.1038/nn1696); pmid: [16648874](https://pubmed.ncbi.nlm.nih.gov/16648874/)
- L. Santarelli *et al.*, Requirement of hippocampal neurogenesis for the behavioral effects of antidepressants. *Science* **301**, 805–809 (2003). doi: [10.1126/science.1083328](https://doi.org/10.1126/science.1083328); pmid: [12907793](https://pubmed.ncbi.nlm.nih.gov/12907793/)
- A. Garthe, J. Behr, G. Kempermann, Adult-generated hippocampal neurons allow the flexible use of spatially precise learning strategies. *PLoS ONE* **4**, e5464 (2009). doi: [10.1371/journal.pone.0005464](https://doi.org/10.1371/journal.pone.0005464); pmid: [19421325](https://pubmed.ncbi.nlm.nih.gov/19421325/)
- C. E. Finch, N. J. Laping, T. E. Morgan, N. R. Nichols, G. M. Pasinetti, TGF-beta 1 is an organizer of responses to neurodegeneration. *J. Cell. Biochem.* **53**, 314–322 (1993). doi: [10.1002/jcb.240530408](https://doi.org/10.1002/jcb.240530408); pmid: [8300749](https://pubmed.ncbi.nlm.nih.gov/8300749/)
- K. C. Flanders, R. F. Ren, C. F. Lippa, Transforming growth factor-betas in neurodegenerative disease. *Prog. Neurobiol.* **54**, 71–85 (1998). doi: [10.1016/S0304-0082\(97\)00066-X](https://doi.org/10.1016/S0304-0082(97)00066-X); pmid: [9460794](https://pubmed.ncbi.nlm.nih.gov/9460794/)
- H. J. Klassen *et al.*, Expression of cytokines by multipotent neural progenitor cells. *Cytokine* **22**, 101–106 (2003). doi: [10.1016/S1043-4666\(03\)00120-0](https://doi.org/10.1016/S1043-4666(03)00120-0); pmid: [12849709](https://pubmed.ncbi.nlm.nih.gov/12849709/)
- Y. Zhu, B. Ahlemeyer, E. Bauerbach, J. Krieglstein, TGF-beta1 inhibits caspase-3 activation and neuronal apoptosis in rat hippocampal cultures. *Neurochem. Int.* **38**, 227–235 (2001). doi: [10.1016/S0197-0186\(00\)00084-X](https://doi.org/10.1016/S0197-0186(00)00084-X); pmid: [11099781](https://pubmed.ncbi.nlm.nih.gov/11099781/)
- D. Battista, C. C. Ferrari, F. H. Gage, F. J. Pitossi, Neurogenic niche modulation by activated microglia: Transforming growth factor beta increases neurogenesis in the adult dentate gyrus. *Eur. J. Neurosci.* **23**, 83–93 (2006). doi: [10.1111/j.1460-9568.2005.04539.x](https://doi.org/10.1111/j.1460-9568.2005.04539.x); pmid: [16420418](https://pubmed.ncbi.nlm.nih.gov/16420418/)
- M. S. Buckwalter *et al.*, Chronically increased transforming growth factor-beta1 strongly inhibits hippocampal neurogenesis in aged mice. *Am. J. Pathol.* **169**, 154–164 (2006). doi: [10.2353/ajpath.2006.051272](https://doi.org/10.2353/ajpath.2006.051272); pmid: [16813639](https://pubmed.ncbi.nlm.nih.gov/16813639/)
- M. Kandasamy *et al.*, TGF-beta signalling in the adult neurogenic niche promotes stem cell quiescence as well as generation of new neurons. *J. Cell. Mol. Med.* **18**, 1444–1459 (2014). doi: [10.1111/jcmm.12298](https://doi.org/10.1111/jcmm.12298); pmid: [24779367](https://pubmed.ncbi.nlm.nih.gov/24779367/)
- F. P. Wachs *et al.*, Transforming growth factor-beta1 is a negative modulator of adult neurogenesis. *J. Neuropathol. Exp. Neurol.* **65**, 358–370 (2006). doi: [10.1097/01.jnen.0000218444.53405.f0](https://doi.org/10.1097/01.jnen.0000218444.53405.f0); pmid: [16691117](https://pubmed.ncbi.nlm.nih.gov/16691117/)

30. S. H. Choi *et al.*, A three-dimensional human neural cell culture model of Alzheimer's disease. *Nature* **515**, 274–278 (2014). doi: [10.1038/nature13800](https://doi.org/10.1038/nature13800); pmid: 25307057
31. J. Cho *et al.*, Treadmill Running Reverses Cognitive Declines due to Alzheimer Disease. *Med. Sci. Sports Exerc.* **47**, 1814–1824 (2015). doi: [10.1249/MSS.0000000000000612](https://doi.org/10.1249/MSS.0000000000000612); pmid: 25574797
32. C. W. Cotman, N. C. Berchtold, Exercise: A behavioral intervention to enhance brain health and plasticity. *Trends Neurosci.* **25**, 295–301 (2002). doi: [10.1016/S0166-2236\(02\)02143-4](https://doi.org/10.1016/S0166-2236(02)02143-4); pmid: 12086747
33. C. W. Cotman, N. C. Berchtold, L. A. Christie, Exercise builds brain health: Key roles of growth factor cascades and inflammation. *Trends Neurosci.* **30**, 464–472 (2007). doi: [10.1016/j.tins.2007.06.011](https://doi.org/10.1016/j.tins.2007.06.011); pmid: 17765329
34. M. Llorens-Martín, I. Torres-Alemán, J. L. Trejo, Growth factors as mediators of exercise actions on the brain. *Neuromolecular Med.* **10**, 99–107 (2008). doi: [10.1007/s12017-008-8026-1](https://doi.org/10.1007/s12017-008-8026-1); pmid: 18286390
35. S. S. Vaynman, Z. Ying, D. Yin, F. Gomez-Pinilla, Exercise differentially regulates synaptic proteins associated to the function of BDNF. *Brain Res.* **1070**, 124–130 (2006). doi: [10.1016/j.brainres.2005.11.062](https://doi.org/10.1016/j.brainres.2005.11.062); pmid: 16413508
36. C. D. Wrann *et al.*, Exercise induces hippocampal BDNF through a PGC-1 α /FNDC5 pathway. *Cell Metab.* **18**, 649–659 (2013). doi: [10.1016/j.cmet.2013.09.008](https://doi.org/10.1016/j.cmet.2013.09.008); pmid: 24120943
37. J. E. Hamos, L. J. DeGennaro, D. A. Drachman, Synaptic loss in Alzheimer's disease and other dementias. *Neurology* **39**, 355–361 (1989). doi: [10.1212/WNL.39.3.355](https://doi.org/10.1212/WNL.39.3.355); pmid: 2927643
38. S. Peng, J. Wu, E. J. Mufson, M. Fahnestock, Precursor form of brain-derived neurotrophic factor and mature brain-derived neurotrophic factor are decreased in the pre-clinical stages of Alzheimer's disease. *J. Neurochem.* **93**, 1412–1421 (2005). doi: [10.1111/j.1471-4159.2005.03135.x](https://doi.org/10.1111/j.1471-4159.2005.03135.x); pmid: 15935057
39. D. T. Proctor, E. J. Coulson, P. R. Dodd, Reduction in post-synaptic scaffolding PSD-95 and SAP-102 protein levels in the Alzheimer inferior temporal cortex is correlated with disease pathology. *J. Alzheimers Dis.* **21**, 795–811 (2010). doi: [10.3233/JAD-2010-100090](https://doi.org/10.3233/JAD-2010-100090); pmid: 20634587
40. P. Rasmussen *et al.*, In humans IL-6 is released from the brain during and after exercise and paralleled by enhanced IL-6 mRNA expression in the hippocampus of mice. *Acta Physiol. (Oxf.)* **201**, 475–482 (2011). doi: [10.1111/j.1748-1716.2010.02223.x](https://doi.org/10.1111/j.1748-1716.2010.02223.x); pmid: 21083649
41. P. C. Baier, U. May, J. Scheller, S. Rose-John, T. Schifflholz, Impaired hippocampus-dependent and -independent learning in IL-6 deficient mice. *Behav. Brain Res.* **200**, 192–196 (2009). doi: [10.1016/j.bbr.2009.01.013](https://doi.org/10.1016/j.bbr.2009.01.013); pmid: 19378383
42. K. K. Bowen, R. J. Dempsey, R. Vemuganti, Adult interleukin-6 knockout mice show compromised neurogenesis. *Neuroreport* **22**, 126–130 (2011). doi: [10.1097/WNR.0b013e3283430a44](https://doi.org/10.1097/WNR.0b013e3283430a44); pmid: 21266900
43. C. A. McPherson, M. Aoyama, G. J. Harry, Interleukin (IL)-1 and IL-6 regulation of neural progenitor cell proliferation with hippocampal injury: Differential regulatory pathways in the subgranular zone (SGZ) of the adolescent and mature mouse brain. *Brain Behav. Immun.* **25**, 850–862 (2011). doi: [10.1016/j.bbi.2010.09.003](https://doi.org/10.1016/j.bbi.2010.09.003); pmid: 20833246
44. L. Vallières, I. L. Campbell, F. H. Gage, P. E. Sawchenko, Reduced hippocampal neurogenesis in adult transgenic mice with chronic astrocytic production of interleukin-6. *J. Neurosci.* **22**, 486–492 (2002). doi: [10.1523/JNEUROSCI.22-02-00486.2002](https://doi.org/10.1523/JNEUROSCI.22-02-00486.2002); pmid: 11784794
45. R. Yirmiya, I. Goshen, Immune modulation of learning, memory, neural plasticity and neurogenesis. *Brain Behav. Immun.* **25**, 181–213 (2011). doi: [10.1016/j.bbi.2010.10.015](https://doi.org/10.1016/j.bbi.2010.10.015); pmid: 20970492
46. C. Zhao, W. Deng, F. H. Gage, Mechanisms and functional implications of adult neurogenesis. *Cell* **132**, 645–660 (2008). doi: [10.1016/j.cell.2008.01.033](https://doi.org/10.1016/j.cell.2008.01.033); pmid: 18295581
47. D. Guerrieri, H. van Praag, Exercise-mimetic AICAR transiently benefits brain function. *Oncotarget* **6**, 18293–18313 (2015). doi: [10.18632/oncotarget.4715](https://doi.org/10.18632/oncotarget.4715); pmid: 26286955
48. T. Kobilo *et al.*, AMPK agonist AICAR improves cognition and motor coordination in young and aged mice. *Learn. Mem.* **21**, 119–126 (2014). doi: [10.1101/lm.033332.113](https://doi.org/10.1101/lm.033332.113); pmid: 24443745
49. X. P. Hong *et al.*, Essential role of tau phosphorylation in adult hippocampal neurogenesis. *Hippocampus* **20**, 1339–1349 (2010). doi: [10.1002/hipo.20712](https://doi.org/10.1002/hipo.20712); pmid: 19816983
50. H. Hörder *et al.*, Midlife cardiovascular fitness and dementia: A 44-year longitudinal population study in women. *Neurology* **90**, e1298–e1305 (2018). doi: [10.1212/WNL.0000000000005290](https://doi.org/10.1212/WNL.0000000000005290); pmid: 29540588
51. S. E. Lamb *et al.*, Dementia And Physical Activity (DAPA) trial of moderate to high intensity exercise training for people with dementia: Randomised controlled trial. *BMJ* **361**, k1675 (2018). doi: [10.1136/bmj.k1675](https://doi.org/10.1136/bmj.k1675); pmid: 29769247
52. A. Santos-Lozano *et al.*, Physical Activity and Alzheimer Disease: A Protective Association. *Mayo Clin. Proc.* **91**, 999–1020 (2016). doi: [10.1016/j.mayocp.2016.04.024](https://doi.org/10.1016/j.mayocp.2016.04.024); pmid: 27492909
53. D. Briley *et al.*, Preserved neurogenesis in non-demented individuals with AD neuropathology. *Sci. Rep.* **6**, 27812 (2016). doi: [10.1038/srep27812](https://doi.org/10.1038/srep27812); pmid: 27298190
54. S. H. Choi *et al.*, Non-cell-autonomous effects of presenilin 1 variants on enrichment-mediated hippocampal progenitor cell proliferation and differentiation. *Neuron* **59**, 568–580 (2008). doi: [10.1016/j.neuron.2008.07.033](https://doi.org/10.1016/j.neuron.2008.07.033); pmid: 18760694
55. M. J. West, H. J. Gundersen, Unbiased stereological estimation of the number of neurons in the human hippocampus. *J. Comp. Neurol.* **296**, 1–22 (1990). doi: [10.1002/cne.902960102](https://doi.org/10.1002/cne.902960102); pmid: 2358525

ACKNOWLEDGMENTS

Funding: Supported by the Cure Alzheimer's Fund (R.E.T. and S.H.C.); the JPB Foundation (R.E.T., B.M.S., and F.H.G.); NIA and NIMH grant 5R01MH060009 (R.E.T.); The Henry and Allison McCance Center for Brain Health at MGH (R.E.T.); NIH/NIA grant 1RF1AG048080-01 (R.E.T. and D.Y.K.); NIH/NIA grant 2R01AG014713 (D.Y.K.); and the Mather's Foundation and the Leona M. and Harry B. Helmsley Charitable Trust (F.H.G.).

Author contributions: R.E.T. and S.H.C. initiated the project; R.E.T. supervised research; R.E.T., S.H.C., F.H.G., H.v.P., and B.M.S. designed experiments; S.H.C., E.B., Z.K.C., C.A., and M.K.O. performed most of the research; S.W.L., G.D.C., and F.H.G. provided LV-Wnt3, LV-dnWnt, and LV-GFP; S.H.C. performed stereotaxic injections; B.P. and J.W.C. performed irradiation; E.B., J.A., and D.Y.K. performed 3D culture experiments; E.K. and A.R. performed Golgi staining, dot-blot, and ELISAs; M.K.O. and A.L. genotyped and maintained mice; C.Z. and S.J.M. performed MSD assays; and S.H.C., E.B., Z.K.C., and R.E.T. wrote the manuscript with editing and input from J.W.C., H.v.P., and F.H.G.

Competing interests: We declare no conflict of interest.

SUPPLEMENTARY MATERIALS

www.sciencemag.org/content/361/6406/eaan8821/suppl/DC1
Figs. S1 to S23
Tables S1 to S10

1 June 2017; resubmitted 4 June 2018
Accepted 17 July 2018
[10.1126/science.aan8821](https://doi.org/10.1126/science.aan8821)

Combined adult neurogenesis and BDNF mimic exercise effects on cognition in an Alzheimer's mouse model

Se Hoon Choi, Enjana Bylykbashi, Zena K. Chatila, Star W. Lee, Benjamin Pulli, Gregory D. Clemenson, Eunhee Kim, Alexander Rompala, Mary K. Oram, Caroline Asselin, Jenna Aronson, Can Zhang, Sean J. Miller, Andrea Lesinski, John W. Chen, Doo Yeon Kim, Henriette van Praag, Bruce M. Spiegelman, Fred H. Gage and Rudolph E. Tanzi

Science **361** (6406), eaan8821.
DOI: 10.1126/science.aan8821

Adult neurogenesis and Alzheimer's disease

Alzheimer's disease (AD) pathology destroys neurons and synapses in the brain, leading to dementia. The brain generates new neurons throughout life in the hippocampus, a process called adult hippocampal neurogenesis (AHN). Choi *et al.* found that blocking AHN exacerbated cognitive impairment in an AD mouse model (see the Perspective by Spire-Jones and Ritchie). Inducing neurogenesis alone did not improve cognition in AD mice, whereas inducing neurogenesis while simultaneously ameliorating the neuronal environment via exercise did. The use of genetic or pharmacological treatments that simultaneously induced neurogenesis and increased levels of brain-derived neurotrophic factor (BDNF) mimicked the benefits of exercise on cognition. Thus, inducing both neurogenesis and providing BDNF may be useful as an AD therapeutic.

Science, this issue p. eaan8821; see also p. 975

ARTICLE TOOLS

<http://science.sciencemag.org/content/361/6406/eaan8821>

SUPPLEMENTARY MATERIALS

<http://science.sciencemag.org/content/suppl/2018/09/05/361.6406.eaan8821.DC1>

RELATED CONTENT

<http://science.sciencemag.org/content/sci/361/6406/975.full>

REFERENCES

This article cites 55 articles, 9 of which you can access for free
<http://science.sciencemag.org/content/361/6406/eaan8821#BIBL>

PERMISSIONS

<http://www.sciencemag.org/help/reprints-and-permissions>

Use of this article is subject to the [Terms of Service](#)